Lab on a Chip

CRITICAL REVIEW

View Article Online
View Journal

Cite this: DOI: 10.1039/c9lc01022j

Computational inertial microfluidics: a review†

Sajad Razavi Bazaz, [a] Ali Mashhadian,‡[b] Abbas Ehsani,‡[c] Suvash Chandra Saha, [d] Timm Krüger[e] and Majid Ebrahimi Warkiani *[af]

Since the discovery of inertial focusing in 1961, numerous theories have been put forward to explain the migration of particles in inertial flows, but a complete understanding is still lacking. Recently, computational approaches have been utilized to obtain better insights into the underlying physics. In particular, fundamental aspects of particle focusing inside straight and curved microchannels have been explored in detail to determine the dependence of focusing behavior on particle size, channel shape, and flow Reynolds number. In this review, we differentiate between the models developed for inertial particle motion on the basis of whether they are semi-analytical, Navier–Stokes-based, or built on the lattice Boltzmann method. This review provides a blueprint for the consideration of numerical solutions for modeling of inertial particle motion, whether deformable or rigid, spherical or non-spherical, and whether suspended in Newtonian or non-Newtonian fluids. In each section, we provide the general equations used to solve particle motion, followed by a tutorial appendix and specified sections to engage the reader with details of the numerical studies. Finally, we address the challenges ahead in the modeling of inertial particle microfluidics for future investigators.

Received 15th October 2019,
Accepted 17th January 2020

DOI: 10.1039/c9lc01022j

rsc.li/loc

[a] School of Biomedical Engineering, University of Technology Sydney, Sydney, New South Wales 2007, Australia. E-mail: majid.warkiani@uts.edu.au
[b] School of Mechanical Engineering, Sharif University, Tehran, Iran
[c] School of Mechanical Engineering, University of Tehran, Tehran, Iran
[d] School of Mechanical and Mechatronic Engineering, University of Technology Sydney, Sydney, NSW 2007, Australia
[e] School of Engineering, Institute for Multiscale Thermofluids, The University of Edinburgh, Edinburgh EH9 3FB, UK
[f] Institute of Molecular Medicine, Sechenov First Moscow State University, Moscow 119991, Russia

† Electronic supplementary information (ESI) available. See DOI: 10.1039/c9lc01022j

‡ These authors contributed equally as the second author.

1 Introduction

Microfluidics, a technology characterized by the engineered manipulation of fluids at the microscale, has shown considerable promise in point-of-care diagnostics and clinical studies.[1] Since its birth in the 1990s, this technology has been matured into a complex field impacting many commercial applications.[2] Isolation, fractionation, and purification of cells using microfluidic platforms have been a flourishing area of development in recent years with many successful translations into commercial products. Several review articles

Sajad Razavi Bazaz

Sajad Razavi Bazaz received his MSc degree as a first rank student in Biomedical Engineering from University of Tehran, Iran, in 2017. He currently holds a position as a PhD candidate in School of Biomedical Engineering at University of Technology Sydney. His main research interest is to investigate fundamentals of inertial microfluidics in hard chips and design and fabricate functional 3D printed inertial microfluidic devices for particles/cells manipulations.

Ali Mashhadian

Ali Mashhadian received his MSc degree in Mechanical Engineering from Sharif University of Technology (STU), Iran, in 2018 with honors and will be pursuing his Ph.D. studies at Cornell University, USA. His research is mainly focused on investigating the fundamental mechanism of inertial focusing in microfluidics channels using direct numerical simulation (DNS) to enhance the performance of inertial-based diagnosis test devices.

are available on particle/cell separation using microfluidics systems, with some of them being presented in ref. 3–5.

Microfluidic systems normally leverage on the disparities in the intrinsic properties of different particle/cell populations (*i.e.*, size, deformability, surface charge, and density) to achieve separations. These systems can be broadly classified as active and passive separation techniques. Active techniques rely on external force fields such as acoustic or magnetic for operation, while passive techniques (*e.g.*, pinched flow fractionation, deterministic lateral displacement (DLD), and inertial microfluidics) rely only on the channel geometry and inherent hydrodynamic forces for functionality.[6] Among all existing microfluidic systems, inertial microfluidics, which takes the advantage of size-dependent hydrodynamic effects in microchannels, has become a promising approach for particle and cell separation due to its capacity in high-volume and high-throughput sample processing.[7–11] Inertial microfluidics has been employed for various applications, influencing a wide range of industries such as microbiology, biochemistry, and biotechnology, most of which can be found in ref. 9, 10 and 12. The most prevalent structures used in inertial microfluidics are demonstrated in Fig. 1A.

Inertial microfluidics is defined as the migration of randomly dispersed particles toward specific equilibrium positions inside a microchannel. This phenomenon was first reported by Segre and Silberberg in 1961.[13] Later, with the advent of microfluidics, it was extensively explored, resulting in numerous articles evaluating the underlying physics of this phenomenon. To date, numerous research groups have attempted to provide a numerical solution to better understand fundamental aspects of particle focusing inside inertial microfluidic systems. These numerical solutions can be divided into three distinct classifications. First, asymptotic analysis by simplification of fluid equations predicts inertial forces acting on a particle within a channel. It has been

Abbas Ehsani

Abbas Ehsani received the BSc degree in mechanical engineering from University of Ferdowsi, Iran, in 2014, and the MSc degree in mechanical engineering from Tehran University, Iran, in 2017. In the same year, he joined Tehran University as a PhD candidate. His current scientific research interest is focused on developing next generation of integrated microfluidic platform for protein detection and purification. Besides, he is perusing his recent investigations on numerical simulation of inertial microfluidics.

Suvash Chandra Saha

Suvash Chandra Saha is a Senior Lecturer of Mechanical Engineering in the School of Mechanical and Mechatronic Engineering, University of Technology Sydney, Australia. He received his PhD in computational fluid dynamics from James Cook University, Australia. Then he undertook postdoctoral training at the Queensland University of Technology, Australia. His current research activities focus on three key areas of (a) computational biomechanical engineering (b) heat and mass transfer, and (c) microfluidic modelling including inertial separation techniques.

Timm Krüger

Timm Krüger is a Lecturer in Chemical Engineering in the School of Engineering at the University of Edinburgh. He specializes in the lattice-Boltzmann modelling and simulation of complex fluids, for example emulsions, suspensions of deformable particles or red blood cells in blood vessels and microfluidic devices. He currently focuses to develop new numerical methods for inertial microfluidics for healthcare applications.

Majid Ebrahimi Warkiani

Majid Ebrahimi Warkiani is an Associate Professor in Biomedical Engineering at University of Technology Sydney. He completed his PhD program at Nanyang Technological University and subsequently undertook postdoctoral training at Singapore-MIT Alliance for Research and Technology (SMART) center. He is NHMRC-CD fellow and also a member of Institute for Biomedical Materials & Devices (IBMD) and Center for Health Technologies (CHT) at UTS. Dr Warkiani's current research activities focus on three key areas of (a) microfluidics (b) organ-on-a-chips, and (c) 3D printing.

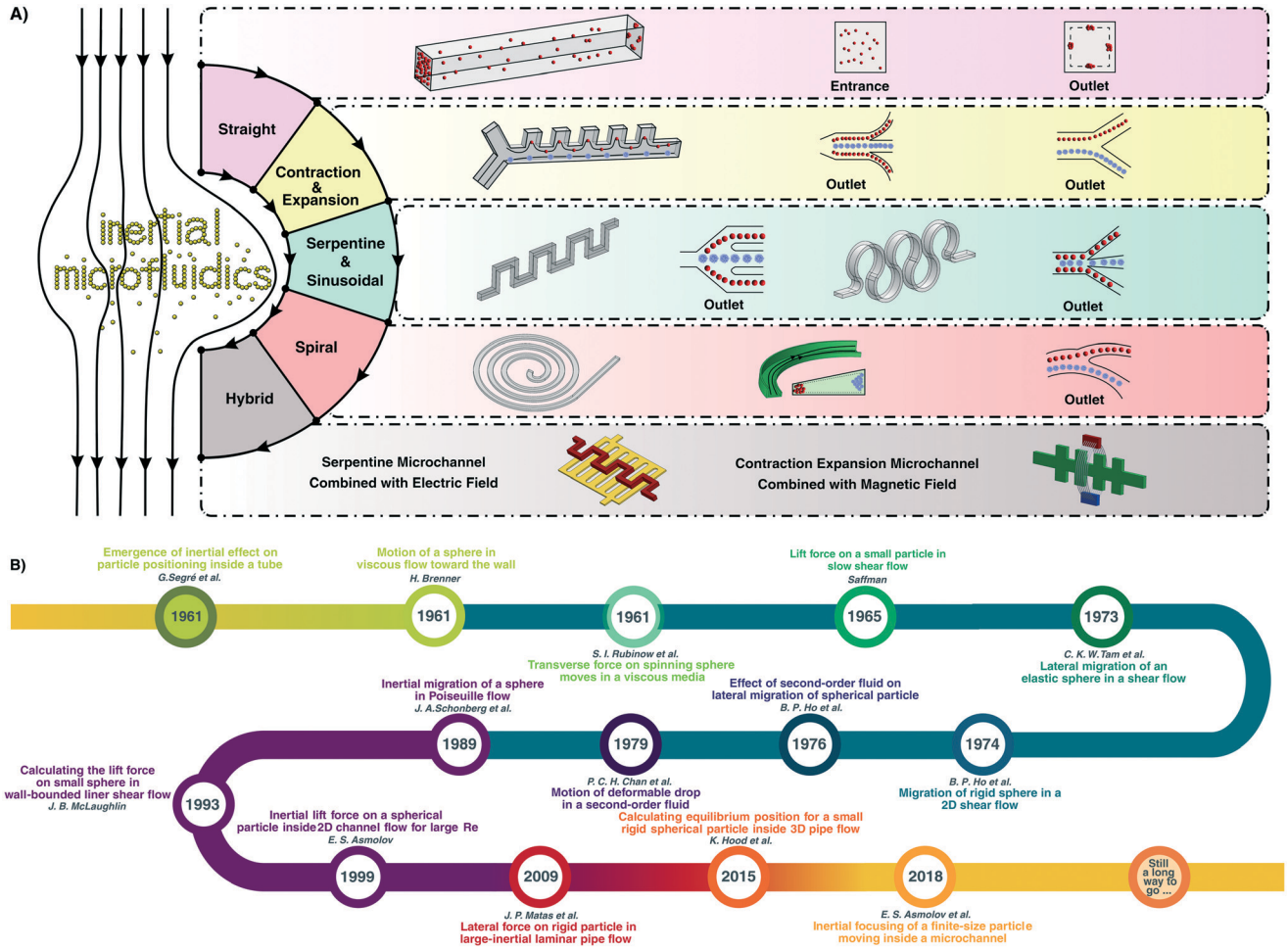

Fig. 1 A) Schematic illustration of various kinds of geometries used for inertial microfluidics. B) Asymptotic solutions for particle migration in confined flow (from early stages to more developed studies).

reported that the phenomena pictured by this solution are far from the real scenario, due to its oversimplifying assumptions and limitations. In the second classification, scientists utilize Navier–Stokes-based solutions for inertial microfluidics, where all prevalent issues of particle size or particle effects on fluid streamline in asymptotic solutions are addressed. However, tracking the solid–fluid interface or the demanding calculation time for solving equations are challenges for Navier–Stokes-based approaches. As an alternative, researchers use the lattice Boltzmann method (LBM) for inertial flow modeling. The relative simplicity of algorithm parallelization, adding new physics, and the strength of LBM in the intermediate Re regime explain its rapidly increasing use for inertial microfluidics over the last decade.

Although numerous review papers exist for inertial microfluidics, there is a lack of a comprehensive review of computational inertial microfluidics. Accordingly, the primary aim of this review paper is to provide researchers with the latest updates regarding computational solutions of inertial particle motion within a microfluidic device. Here, we have reviewed all computational attempts for inertial particle motion, covering asymptotic calculations, Navier–Stokes-based approaches, and LBM.

2 Asymptotic solutions

In 1961, Segre and Silberberg demonstrated that a suspension of neutrally buoyant particles flowing in a tube with radius R migrate to positions $0.6R$ from the centerline when inertial forces are dominant.[13–15] Since then, many attempts have been made to justify this observation or establish a new theory or method to predict this phenomenon. These methods are summarized in Fig. 1B.

The asymptotic solutions are among the early attempts made for predicting particle migration in confined and non-confined flows. Despite their weakness to capture specific details, such as the particle–fluid interaction and disturbed fluid velocity profiles around the particle, and to apply to a complex 3D domain, these solutions are convincing enough to explain the phenomenon in the most time-efficient manner.

In 1961, Brenner investigated the motion of a particle toward a semi-infinite plane surface.[16] The effect of the plane

surface is considered using two distinct cases: a rigid plane surface and a free plane surface. They found that resistance against a particle path increases in a wall-bounded case (*e.g.*, particle motion within a confined channel) compared to an unbounded case (*e.g.*, particle movement in an infinite fluid domain) when a particle moves under otherwise identical conditions. Nowadays, we know that a particle experiences more resistance along its way near the walls. The results obtained for a solid surface or a free plane surface resulted in a drag force (F_d) on the sphere which is shown by eqn (1) and (2):

$$F_d = 6\pi\mu bU\left\{\frac{4}{3}\sinh(\alpha)\sum_{n=1}^{\infty}\frac{n(n+1)}{(2n-1)(2n+3)}\left[\frac{2\sinh(2n+1)\alpha+(2n+1)\sinh 2\alpha}{4\sinh^2\left(n+\frac{1}{2}\right)\alpha-(2n+1)^2\sinh^2\alpha}-1\right]\right\} \quad (1)$$

$$F_d = 6\pi\mu bU\left\{\frac{4}{3}\sinh(\alpha)\sum_{n=1}^{\infty}\frac{n(n+1)}{(2n-1)(2n+3)}\left[\frac{4\cosh^2\left(n+\frac{1}{2}\right)\alpha+(2n+1)^2\sinh^2\alpha}{2\sinh(2n+1)\alpha-(2n+1)\sinh(2\alpha)}-1\right]\right\} \quad (2)$$

where U is the fluid velocity, μ is the fluid viscosity, and α is a term that relates the ratio of sphere radius (b) to the distance of its surface from the plane (h), as shown by eqn (3).

$$\alpha = \cosh^{-1}\left(\frac{h}{b}\right) = \ln\left\{\frac{h}{b}+\sqrt{\left[\left(\frac{h}{b}\right)^2-1\right]}\right\} \quad (3)$$

In another work, the force exerted on a spinning particle moving in a viscous fluid was investigated using a combination of Stokes and Oseen expansions.[17] Since both expansions are for the same solution and each is valid over its own range, the idea was that these two expansions should be matched at the interface. Through the mathematical derivations, lift and drag forces over the particle were extracted as by eqn (4) and (5), respectively.

$$F_l = \pi a^3\rho\Omega \times V\left[1 + O(\mathrm{Re})\right] \quad (4)$$

$$F_d = -6\pi a\mu V\left[1+\frac{3}{8}\mathrm{Re}+o(\mathrm{Re})\right] \quad (5)$$

where ρ is the fluid density, Ω is the angular velocity of the particle, a is the particle diameter, and V is the relative velocity between fluid and particle. These two formulas are acceptable for a moving particle in an initially quiescent flow. The transverse force on a particle in a 3D Poiseuille flow was calculated based on eqn (6).

$$F_l = -2\pi a^5\rho {U_0}^2 b/3{R_0}^4 \quad (6)$$

where R_0 is the radius of the tube. Eqn (6) shows a force in the direction of the central axis where the force vanishes; however, since the Segre and Silberberg observations[13,18] show that particles tend to concentrate on an annulus of a tube, this formula requires further development and modification.

These studies were further continued by Saffman[19] who showed that if a spherical particle travels through a highly viscous liquid with the velocity (V) relative to a uniform and simple shear flow, it will encounter a lift force perpendicular to both rotational and translational velocity vectors. If the particle lags behind the fluid with a relative velocity, fluid would push the particle toward the center, and *vice versa*. This force can be calculated by eqn (7).

$$F = \frac{81.2\mu V a^2\zeta^{0.5}}{\nu^{0.5}} \quad (7)$$

here, ζ is the magnitude of the velocity gradient. This model was valid only when there was a difference between fluid and particle velocity. Besides, the effect of the wall on the velocity profile around the particle was omitted by the assumptions of this model. As a result, this model was unable to resolve the motion of particles near the wall.

Lateral force on a deformable sphere in an inertia-less steady shear flow was observed by Tam and Hyman.[20] A rigid particle does not experience any lift force in a creeping flow; however, a deformable particle is affected even in a Stokes flow regime. To characterize the deformation of a particle, it was assumed that the elastic displacement was sufficiently small; hence, the linear elastic theory was used, and the total transverse force was obtained as eqn (8).

$$D_y = 4\pi\left[\frac{9\mu a}{20}U_\infty C_{21}^1 - 5\mu a^2\omega\left(\frac{\frac{27}{20}\mu U_\infty}{aG\left(2+\frac{\lambda}{G}\right)}+aB_{10}^1\right)\right] \quad (8)$$

C_{21}^1 and B_{10}^1 are constant parameters that are available in ref. 20, and λ and G are Lamé constants.

Through particle tracking analysis, it was shown that particles reached an equilibrium position for both simple shear and Poiseuille flow, independent of the initial particle position, where particles reside on the centerline for simple shear flow and 0.3 times half the channel height for Poiseuille flow for $\mathrm{Re} \ll 1$. Moreover, a general lateral force (eqn (9)) was proposed, in which k is the ratio of the particle diameter to the channel height, β is $4U_{max}(1-2s)$ for Poiseuille flow and U_{wall} for simple shear flow, γ is the shear rate, and G_1 as well as G_2 are numerically predefined functions in terms of s, which is illustrated in Fig. 2.[21]

$$F_L = k^2\mathrm{Re}(\beta^2 G_1(s) + \beta\gamma G_2(s)) \quad (9)$$

Also, it has been illustrated that rigid particles ($a \ll H$) in a second-order fluid (a well-known viscoelastic fluid model)

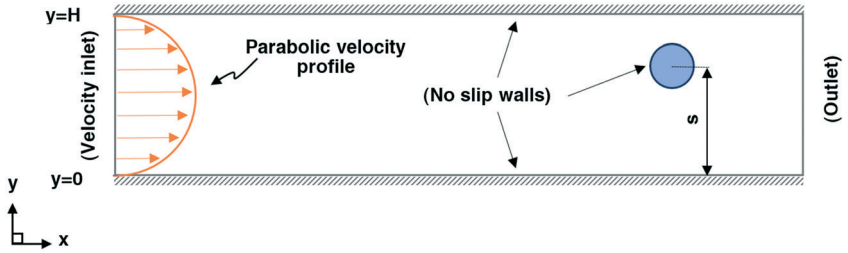

Fig. 2 The schematic view of a cylindrical particle inside the confined channel flow.

migrated toward the centerline due to the induced force from normal stress differences in Poiseuille flow, and toward the outer cylinder in the case of circular Couette flow.[22] When the ratio of Weissenberg number (Wi) to Re is much more than unity (Wi/Re $\gg$ 1), the effect of inertial terms in the Navier–Stokes equations are negligible (creeping flow limit), and thus non-Newtonian effects are dominant. Eqn (10) shows the reported explicit form of lift force in the case of Poiseuille flow.

$$F_L = -\frac{80}{3}\pi k^3 {V_{Max}}^2 (1-2s)(N_1 - 2N_2) \quad (10)$$

where k is the blockage ratio, N_1 and N_2 are the first and second normal stress differences, respectively, and s is normalized vertical location of the particle inside the domain (Fig. 2).

In 1989, Schonberg *et al.* presented that in a 2D Poiseuille flow, by increasing Re, particles tend to migrate toward the wall.[23] However, the particle was assumed to be small enough so that the velocity profile inside the channel remains undisturbed, indicating that the particle Re $\ll$ 1. The singular perturbation technique was employed to solve coupled flow and particle equations in this article. It is demonstrated that the particle equilibrium position becomes closer to the wall as Re increases, which was validated with experimental data of Segre and Silberberg.[13]

The majority of studies so far have dealt with particle migration in the small and intermediate Re flow regime (Re $<$ 3000). However, in 1999, Asmolov investigated the lateral migration of buoyant and non-buoyant particles in 2D confined flow over a wide range of Re and presented some results for unbounded and semi wall-bounded cases.[24] It was shown that two equilibrium positions exist for neutrally buoyant particles. It was mentioned that net inertial lift force exerted on the neutrally buoyant particle in 2D Poiseuille flow could be determined using eqn (11), where c_l is the lift coefficient that is a function of particle lateral position and Re, ρ_f is the fluid density, G is the local shear rate, and a is the particle diameter.

$$F_L = c_l \rho_f G^2 a^4 \quad (11)$$

While many studies have addressed the migration of particles in planar fluid flow, it is crucial to investigate the effect of a realistic 3D fluid flow on particle migration in confined flow. To address this issue, Matas and his colleagues were one of the pioneers who analyzed 3D particle inertial migration over a wide range of Re (1–2000) in a pipe flow.[25] Accordingly, the matched asymptotic expansion was used for cylindrical pipe flow, which was previously used for the planar case.[24] Based on their results, lift force in a pipe flow was qualitatively similar but quantitatively different from the one in a planar channel flow. Furthermore, the equilibrium position of particles in the planar flow was closer to the wall, and the magnitude of the lift force in planar flow was considerably larger than that of pipe flow. For Re $>$ 700 and in the case of pipe flow, one additional equilibrium position exists.[26]

Previous matched asymptotic solutions and point particle methods assumed that the particle is small enough to not disturb the fluid flow. However, particle size has a vital role in particle migration. Therefore, these methods cannot fully capture the particle trajectory. To meet this demand, Hood *et al.* developed a new theory for the exerted force on finite-size particles within a 3D microchannel flow with a square-shaped cross-section.[27] They employed a numerical method to analyze the dominant balancing forces within the Navier–Stokes equations and then derived an asymptotic model to calculate the lift force on spherical particles as a function of their particle size. Their results were valid up to Re of 80, with maximum particle size being limited only by the proximity of the particles to the walls. Furthermore, they illustrated that the lift force tended to zero at eight symmetrically points around the microchannel section, while four points were stable, but the others were unstable. This observation was in good agreement with the experimental data.[27] Earlier in 2018, Asmolov *et al.* developed a new theory for the lift force on finite-size particles in a confined microchannel flow for Re $<$ 20.[28] They showed that this theory might be applicable for the use beyond Re of 20 and other confined flows such as pipe flow. The predicted results obtained from their new model were verified by LBM. The proposed lift force is defined by eqn (12).

$$F_L = \rho a^4 {G_m}^2 \left(C_0\left(\frac{z}{H}\right) + \gamma C_1\left(\frac{z}{a}\right) V_s + C_2\left(\frac{z}{a}\right) {V_s}^2\right) \quad (12)$$

where a is the particle radius, G_m is the maximum shear rate at the wall, V_s is slip velocity, and C_i values are listed as follows.

$$C_0\left(\frac{z}{H}\right) = 2.25\left(\frac{z}{H} - 0.5\right) - 23.4\left(\frac{z}{H} - 0.5\right)^3 \quad (13)$$

$$C_1\left(\frac{z}{a}\right) = -3.24139\frac{z}{a} - 2.676 - 0.8248\left(\frac{z}{a}\right)^{-1} + 0.4616\left(\frac{z}{a}\right)^{-2} \quad (14)$$

$$C_2\left(\frac{z}{a}\right) = 1.7631 + 0.3561\left(\frac{z}{a}\right)^{-1} - 1.1837\left(\frac{z}{a}\right)^{-2} + 0.845163\left(\frac{z}{a}\right)^{-3} \quad (15)$$

This study proposed one of the first models for inertial migration of finite-sized particles in confined microchannel fluid flow. In particular, this model shows a remarkable increase in the lift force near the walls.

3 Navier–stokes-based solutions

Semi-analytical and asymptotic solutions based on perturbation theories can explain the physics of particle motion since they provide an explicit formula for the forces acting on the particle.[29–31] However, these methods have some restrictions that limit their application to a variety of scenarios. These restrictions include particle size, Re, and the distance between the particle and the wall.[32–35] There are many cases of particle motion that do not comply with these restrictions.[36–38] For these cases, numerical methods are powerful alternatives that can determine the motion of particles for a wide range of sizes and Re.[39] Most existing commercial CFD packages employ the point particle assumption when simulating particle motion. Since there is not an exact formula for calculating inertial lift forces acting on a particle, these packages cannot predict the particle trajectory in inertial flows precisely. DNS can be considered as an alternative and robust method, in which forces acting on a particle are calculated from the interaction between the fluid and the particle. The most frequently used methods, which adopt DNS to simulate particulate motion, are briefly explained in the following.

3.1. Most common numerical methods for inertial particulate flows

3.1.1 Flow at specific particle position (FSPP). In some studies, the steady-state flow around the particle and inertial forces acting on the particle at a specific point have been studied, obviating the need for calculating the whole particle trajectory. Accordingly, in 2009, Di Carlo[40] proposed a DNS method for calculating the steady-state flow fields around a single particle at specific positions of the channel cross-section to obtain the net inertial force acting on a particle. This method is highly efficient as it avoids problems encountered in the calculation of transient particle motion such as remeshing at each time step. To calculate the steady-state flow field around a single particle in the position (y,z) of the channel cross-section (Fig. 3A), a part of the channel with sufficient length should be considered (usually $20a$ is adequate for neglecting the effect of the particle–particle interaction, where a is the diameter of the particle). Then, the particle is located at the center of this part at position (y,z). The boundary conditions shown in Table 1 are implemented in the channel.

In the beginning, the particle is considered to be at rest. Using continuity and Navier–Stokes equations (eqn (16) and (17)), pressure and velocity fields around the particle are calculated. Next, the values of the forces and torques exerted on the particle are obtained. Translational and angular velocities of the particle are calculated *via* Newton's second law (eqn (18) and (19)).

$$\nabla\cdot u = 0 \quad (16)$$

$$\rho\left(\frac{\partial u}{\partial t} + (u\cdot\nabla)u\right) = -\nabla p + \eta_s\nabla^2 u \quad (17)$$

$$m_p\frac{du_p}{dt} = \oint_{\partial V_p}\left[-PI + \eta_s\left(\nabla u + \nabla u^T\right)\right]\cdot n\,dS \quad (18)$$

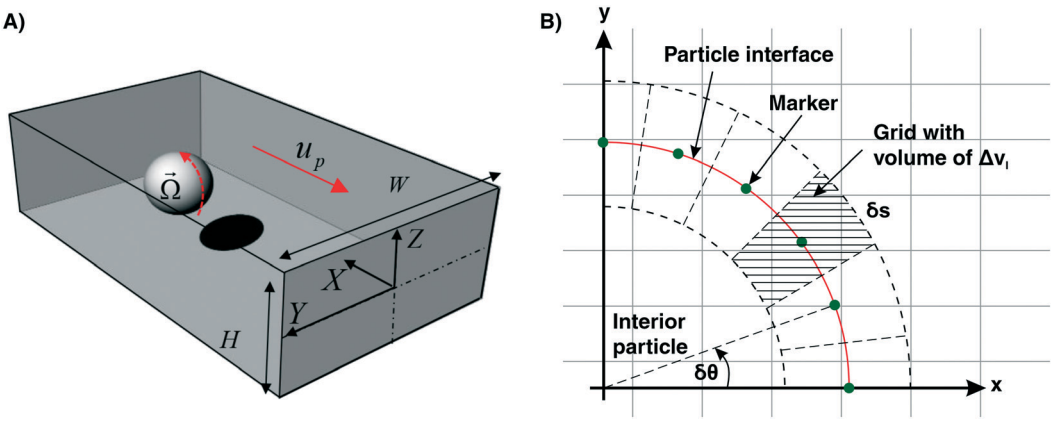

Fig. 3 A) Schematic illustration of particle motion in a part of the channel. The surface of particle rotates with an angular velocity of Ω, and walls have the backward velocity of u_p. Reprinted from ref. 50 with the permission of AIP Publishing. B) Representation of the Eulerian and distribution of Lagrangian grids. Eulerian grid is shown with fix staggered Cartesian grid with gray color. Lagrangian gird is represented by a set of green markers, which are distributed evenly over the surface of the particle with an element size of Δv_l.

Table 1 Boundary condition of the particle for FSPP method

Boundary	Boundary condition
Inlet	Fully developed laminar flow
Outlet	Fully developed laminar flow
Walls	Moving wall
Particle surface	No slip

$$I_p \frac{d\Omega_p}{dt} = \oint_{\partial V_p} r \times \{[-PI + \eta_s(\nabla u + \nabla u^T)]\cdot n\} dS \quad (19)$$

In these equations, ∂V_p and n are the particle surface and outward unit normal vector, respectively. At the next time step, values of the boundary conditions are updated by velocities obtained from the previous time step, and the flow field is solved again. This iterative algorithm is terminated when the momenta in y and z directions and the force F_x per surface area of the particle become smaller than a specified value. Finally, components of the inertial lift force acting on the particle in the y–z plane, *i.e.*, F_y and F_z at point (y_1, z_1) are calculated. By repeating this process for different positions of the channel cross-section, the distribution of inertial forces in the cross-section of the channel can be obtained.

3.1.2 Arbitrary Lagrangian–Eulerian (ALE) method. In the ALE method proposed by Hughes *et al.*,[41] the system of suspended rigid particles in an incompressible fluid flow is considered. The surface velocity of each particle is $u = u_p + \Omega_p \times (x - x_p)$. Here, u_p, Ω_p, and x_p are the particle's center velocity, angular velocity, and center position, respectively. Fluid flow is solved using incompressible continuity and Navier–Stokes equations. In most studies, a finite element scheme is used for solving the flow. At the next time step, particle positions, orientations, and their velocities are updated by integrating the total stress on the surface of each particle and Newton's second law (eqn (18) and (19)). A new mesh should be generated at this time step to recalculate the flow field. Using this iterative solution, one can track the particle trajectories at each time step. The difficulty of this method is updating the mesh at each time step, which is a time-consuming process. In this method, if the density of a particle is less than that of the fluid, the above explicit time-stepping method leads to an unstable solution. This instability can be overcome by separating part of the drag force, which contributes to the acceleration of fluid around the particles from the total drag force.[42] For more information about the ALE method and methods for stabilizing its solution, readers can refer to ref. 43.

3.1.3 Fictitious domain methods. As stated in the ALE method, the computational domain is re-meshed at each time step when particles move along the domain. In fictitious domain methods, a fixed mesh is used for the simulation of particulate flows. Unlike the ALE method, this mesh includes the domain inside the particles, and the flow field is solved for the entire computational domain using the Navier–Stokes equations. Moreover, to ensure that the fluid inside each particle obeys the rigid body motion, a force is applied to its domain. Fictitious methods are classified according to this applied force. If this force is applied to the surface of the particle, it is called the immersed boundary method (IBM), while if it is applied to the body of the particle, it is called the immersed body method. Here, we only describe the distributed Lagrange multiplier (DLM) method as a subset of the immersed body method that is frequently used for simulation of particle motion in inertial microfluidics.

Distributed Lagrange multiplier (DLM). The DLM method is an immersed body type of the fictitious domain method introduced by Glowinski *et al.*[44] in the framework of the finite element method. In summary, to solve the flow, one mesh for the pressure field and one finer mesh for the fluid velocity field are required. Particle domains are discretized with additional meshes, which move with their corresponding particles. The size of the fluid mesh should be smaller than that of the particle mesh to avoid the overestimation of the system. The flow field is solved over the whole computational domain, including the particles' interior. A distribution of Lagrange multipliers as body force densities is used to force the flow inside the particles to show a rigid body motion. The value of the Lagrange multipliers is calculated using the constraint $u = u_p + \Omega_p \times (x - x_p)$ at each point of the mesh inside the particle. For more details about this method, please refer to ref. 43.

Immersed boundary method (IBM). In IBM, there are two computational grids.[45–49] The first one, which is for the fluid, is a fix staggered Cartesian grid which is referred to as the Eulerian grid. The second grid is represented by a set of markers, $X_l \ \forall \ 1 \le l \le N$, which distribute evenly over the surface of the particle. This set is referred to as the Lagrangian grid (Fig. 3B). Each of markers has an element size of Δv_l and the marker locates at the center of this element. Since in the IBM, the no-slip boundary condition is not imposed at the surface of the particle explicitly, a force distribution should be defined on the particle's surface and added to the Navier–Stokes equation to guarantee the constrained rigid motion of the particle. Moreover, because there are two different grids, the value of force and velocity between Eulerian and Lagrangian grids should be transferred using interpolation based on the regularized Dirac delta function $\delta_h(x)$.[45] To calculate the force distribution, first, the velocity predicted on the Eulerian grid is interpolated at Lagrangian markers (eqn (20)). Second, the forces on the Lagrangian mesh are computed based on the difference between the interpolated velocity and the particle velocity. Third, this force is spread to the Eulerian grid (eqn (21)). Finally, this force in Eulerian grid is added to the Navier–Stokes equation to calculate the flow field and the motion of particles using Newton's second law.[45,46]

$$u(X_l, t) = \sum_{ijk} u_{ijk}(x_{ijk}, t)\delta_h(x_{ijk} - X_l)\Delta x \Delta y \Delta z \quad (20)$$

$$f(x_{ijk}, t) = \sum_l \rho \frac{U_p(X_l, t) - u(X_l, t)}{\Delta t}\delta_h(x_{ijk} - X_l)\Delta v_l \quad (21)$$

3.2. Particle motion in Newtonian fluid flow

3.2.1 Straight channels

Particle motion in a tube and Couette flow. The first attempts to numerically investigate particle motion in a shear flow was made by Feng *et al.*[36] They considered neutrally and non-neutrally buoyant particle motion in 2D horizontal Couette and Poiseuille flows, which was followed by similar studies for 3D cases.[51] These studies used the ALE method for the simulation of particle motion and illustrate that the density difference between particle and fluid plays a crucial role in the lateral equilibrium position of particles.

Similarities in the particle motion between confined and unconfined flows motivate several groups to propose lift formulas analogous to the lift force formula acting on a particle in classical aerodynamics using ALE[39,52] and DLM methods.[39] In these studies, since the motion of a single particle was investigated, ALE method was a better choice to obtain more precise results than DLM.

Shao *et al.*[37] investigated particle motion in a tube at different Re by introducing some modifications to the DLM method. They found that by an increase in Re, the equilibrium position shifts from the Segre and Silberberg equilibrium position to the inner radius equilibrium position (Fig. 4A). The critical Re in which the inner equilibrium position becomes stable is a function of the particle size and the distance between each particle in the flow direction.

Particle motion in channels with a rectangular cross-section. The physics of inertial microfluidics in channels with rectangular cross-sections is more complicated compared to tubular flows. Liu *et al.*[38] and Mashhadian and Shamloo[53] investigated the migration of particles in a straight channel with a rectangular cross-section using the FSPP method. Particle migration in this channel can be divided into two steps. First, particles enter the channel at random positions (Fig. 4BI) and focus in a line around the walls (Fig. 4BII). Vectors in Fig. 4B show the direction of particle movements. Second, particles move slowly on the black dashed line to reach their equilibrium positions (Fig. 4BIII).

Experimental results of different studies illustrate various focusing patterns at the outlet of the channel.[54,55] To address these diversities, several researchers numerically investigated the migration of particles in straight rectangular channels.[38,40,53,56,57] Hence, the value of inertial lift force (F_L) at different positions within the cross-section should be investigated. Here, F_L acting on the particle in a rectangular channel is a function of particle size (a), the aspect ratio of the cross-section (AR), Re, and the position of the particle in the channel cross-section. Di Carlo and his colleagues[40] were pioneers in investigating the distribution of the inertial lift force in the cross-section of square channels using the FSPP method (Fig. 5AI). The value of the lift force acting on particles in the horizontal direction (x-direction) from the center to the wall is depicted in Fig. 5AII. The positive and negative values of F_L denote that the direction of the lift force is toward the wall and toward the channel center, respectively. The point at which the F_L curve has a value of zero while its slope is negative is a stable equilibrium position in that direction (Fig. 5AII, red circle). Due to the symmetry of the channel cross-section, all four positions near the center of each wall are stable (Fig. 5A and B).[40,56,57] Fig. 5B is obtained using numerical simulation with a combination of the discrete element method and the immersed boundary method (DEM/IBM). Fig. 5C presents the nondimensional lift force acting on the particle in a square channel from the center of the channel to the wall, which is calculated using the FSPP method for three different sizes of the particle at a constant Re. By increasing the particle size, the equilibrium position approaches the channel center,[57] while by increasing Re, this equilibrium position moves toward the wall.[40] Also, in rectangular channels, depending on Re, there are several equilibrium positions near the channel walls.[38,53] At low Re, the equilibrium positions at the center of long walls are stable (Fig. 5DI). By increasing Re, the equilibrium positions near the center of short walls also become stable (Fig. 5DII). Moreover, if Re increases to high values, new equilibrium positions emerge near the long walls (Fig. 5DIII and BII).

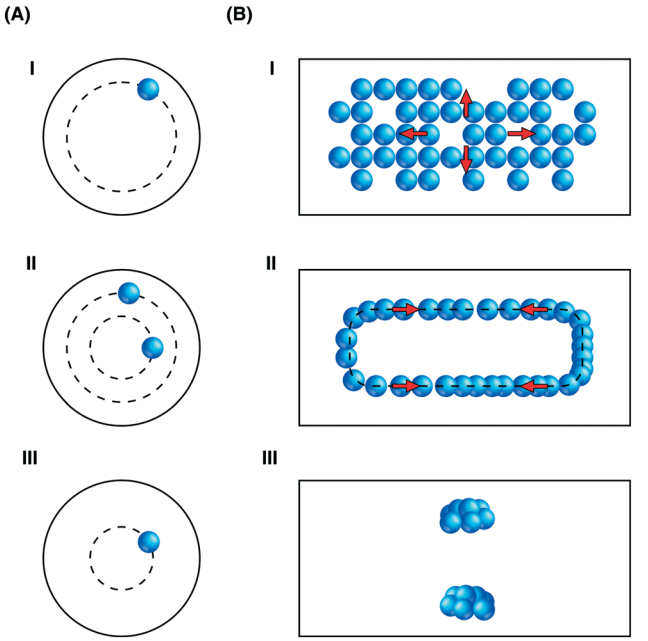

Fig. 4 A) Three different modes of equilibrium positions in a tube flow.[37] I) Re of the channel is under critical Re and all of the particles reach equilibrium position on Segre and Silberberg equilibrium circle (mode I). II) Re is in the transition regime, and particles that are close to the channel axis are focused at the inner equilibrium position (mode II). III) At high Re, all particles reach an equilibrium position at the inner equilibrium position (mode III). B) Migration of particles in straight rectangular channels. I) Schematic of initial particle positions at the inlet of the channel. II) Particles line on a periphery near the channel walls. III) Particles move slowly toward equilibrium positions and reach equilibrium at the center of long walls.

Effect of the particle on fluid flow. In the majority of studies on particulate flows, the effect of fluid on the particle has been investigated to trace the particle migration. However, there are limited works investigating the effect of particles on the carrier fluid, which is of utmost importance to fully

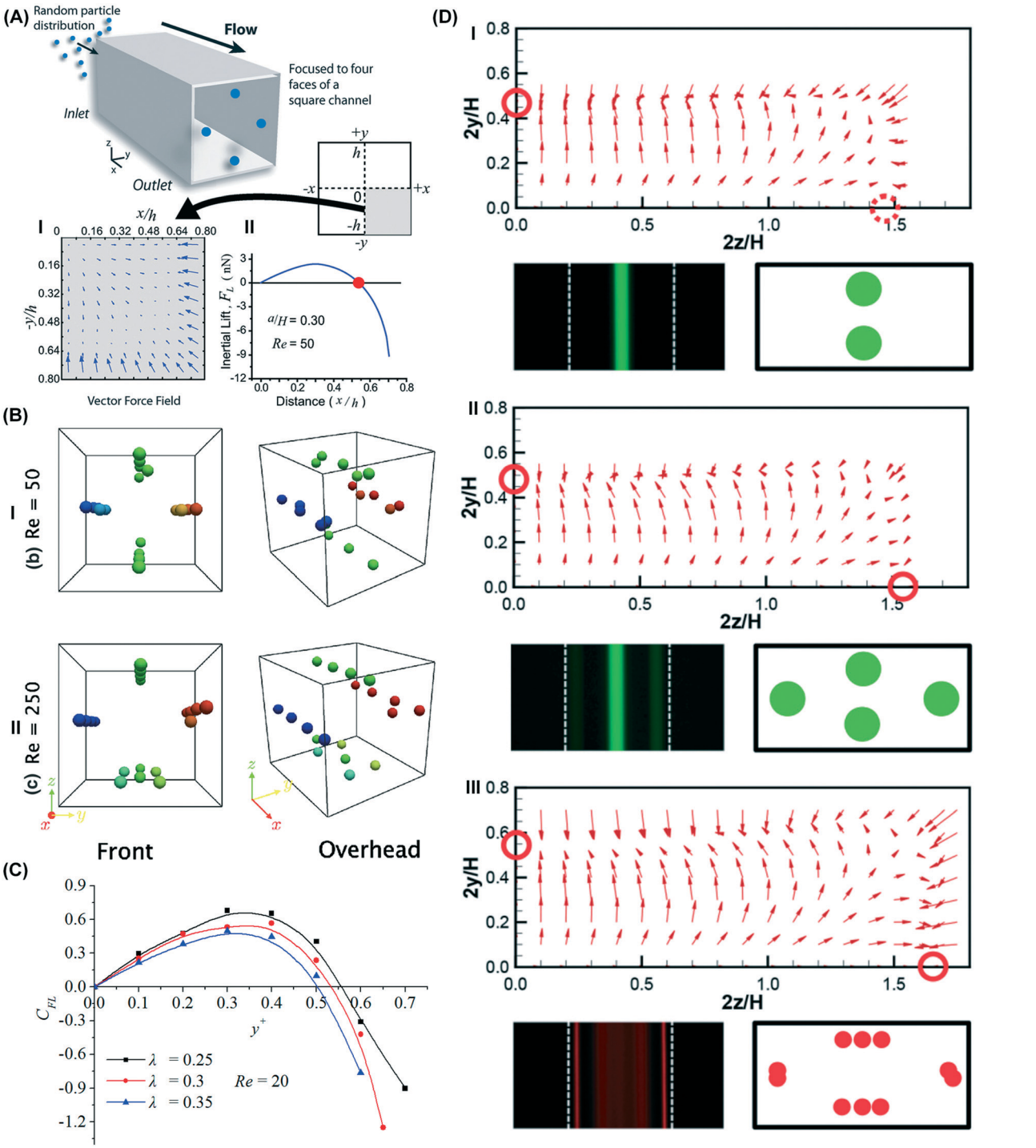

Fig. 5 Inertial microfluidics in the straight channels with rectangular and square cross-sections. A) The lift force acting on the particle in a square channel. Reproduced from ref. 10 with permission from The Royal Society of Chemistry. I) Distribution of the lift force in a quarter of the cross-section. II) Value of inertial lift force from the center to the wall. I and II are reprinted from ref. 40 with permission from the American Physical Society, Copyright 2009. https://doi.org/10.1103/PhysRevLett.102.094503. B) The focusing pattern of particles in a channel with a square cross-section at low (I) and high (II) Re. Reprinted from ref. 56 with the permission from the Springer. C) By increasing the particle size (blockage ratio), the equilibrium position of particle moves toward the center. Reproduced from ref. 57 with permission under open license CC BY 4.0. D) Distributions of lift force acting on the particle in a rectangular channel with an aspect ratio of two under various Re and particle sizes. Reproduced from ref. 38 with permission from The Royal Society of Chemistry. I) Only the centers of the long walls are stable equilibrium positions (the blockage ratio (a/H) = 0.3 and Re = 100). II) Stable equilibrium particle position at Re = 200 and blockage ratio of 0.3 III) by increasing Re to high values (Re = 200) for the blockage ratio (a/H) = 0.1, new equilibrium positions emerged near the centers of long walls.

understand the exact mechanism of particle focusing within inertial microfluidic systems.[58–60]

Confined particulate flows show some distinguishable behaviors in comparison to those in the open boundary shear flows. In an inertia-less open boundary shear flow (*i.e.*, Stokes flow), two kinds of streamlines relative to the particle velocity, namely closed and open streamlines, exist (Fig. 6A). Streamlines in the vicinity of the particles spiraling around them and the vorticity axis are called an area with closed streamlines.[58] On the other hand, outside the closed streamline area, the open streamline area can be observed where streamlines after passing the obstacle return to their previous directions. Moving to an inertial regime causes the closed streamlines around the particle to collapse. This creates two reversed streamline areas (Fig. 6B). Both the spiraling streamline and reversed streamline areas meet each other at a stagnation point.[61] Fig. 6A and B are obtained *via* numerical simulations using the front-tracking finite difference method.[58]

Unlike open boundary shear flows, reversed streamlines are observed in confined particulate flows in the Stokes regime (Fig. 6C).[59] The distribution of streamlines relative to the particle velocity around a particle in confined inertial flows is similar to that in open boundary flows; however, in confined flows, the symmetry present in open boundary shear flows (in the vertical direction) does not exist, owing to the parabolic nature of the flow (Fig. 6D). Fig. 6C and D are examples of an FSPP-based simulation.

A secondary flow in the channel cross-section is generated once there is a particle in the channel, even the particle has no rotation and is located at the channel center.[60] Fig. 6E, obtained through the FSPP method, represents the value and direction of secondary flows created due to the presence of a

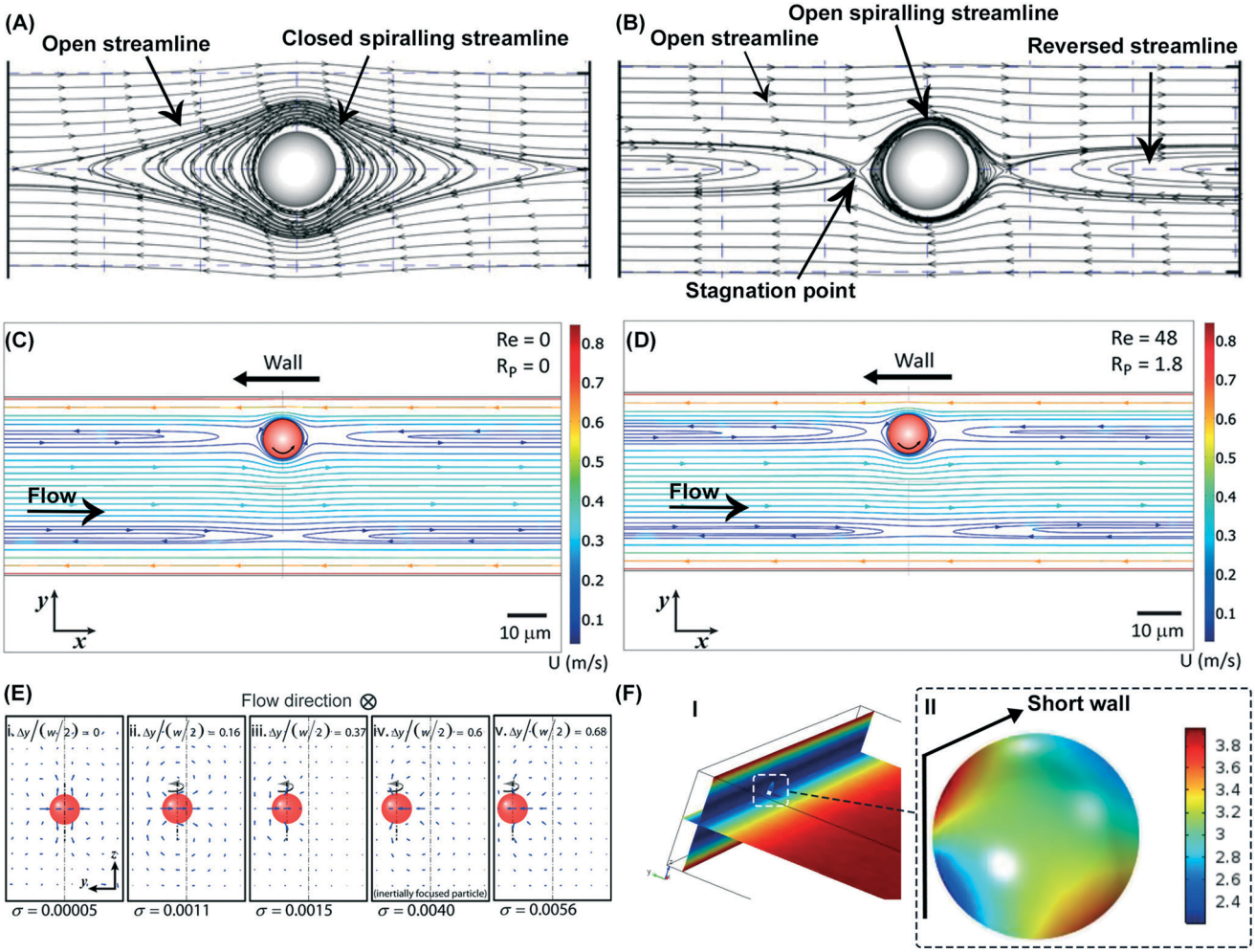

Fig. 6 Distribution of streamlines around a particle in an open boundary shear flow. A) Closed streamline areas near the particle in Stokes flow and B) reversed streamline areas around the particle in the inertial flow. Reproduced with permission from ref. 58. Distribution of streamlines relative to particle velocity around a moving particle in confined flow. Reversed streamline observed in both C) inertia-less and D) inertial flow regimes. Reproduced from ref. 59 with permission from the National Academy of Sciences, Copyright 2010. E) The lateral position of the particle in the cross-section of the channel has a significant impact on the strength and direction of induced secondary flows. Reproduced from ref. 60 with permission from the National Academy of Sciences, Copyright 2012. F) I. Isometric view of the velocity distribution. II. Top view of pressure distributions on the surface of the particle near the wall. Reprinted from ref. 50 with the permission of AIP Publishing.

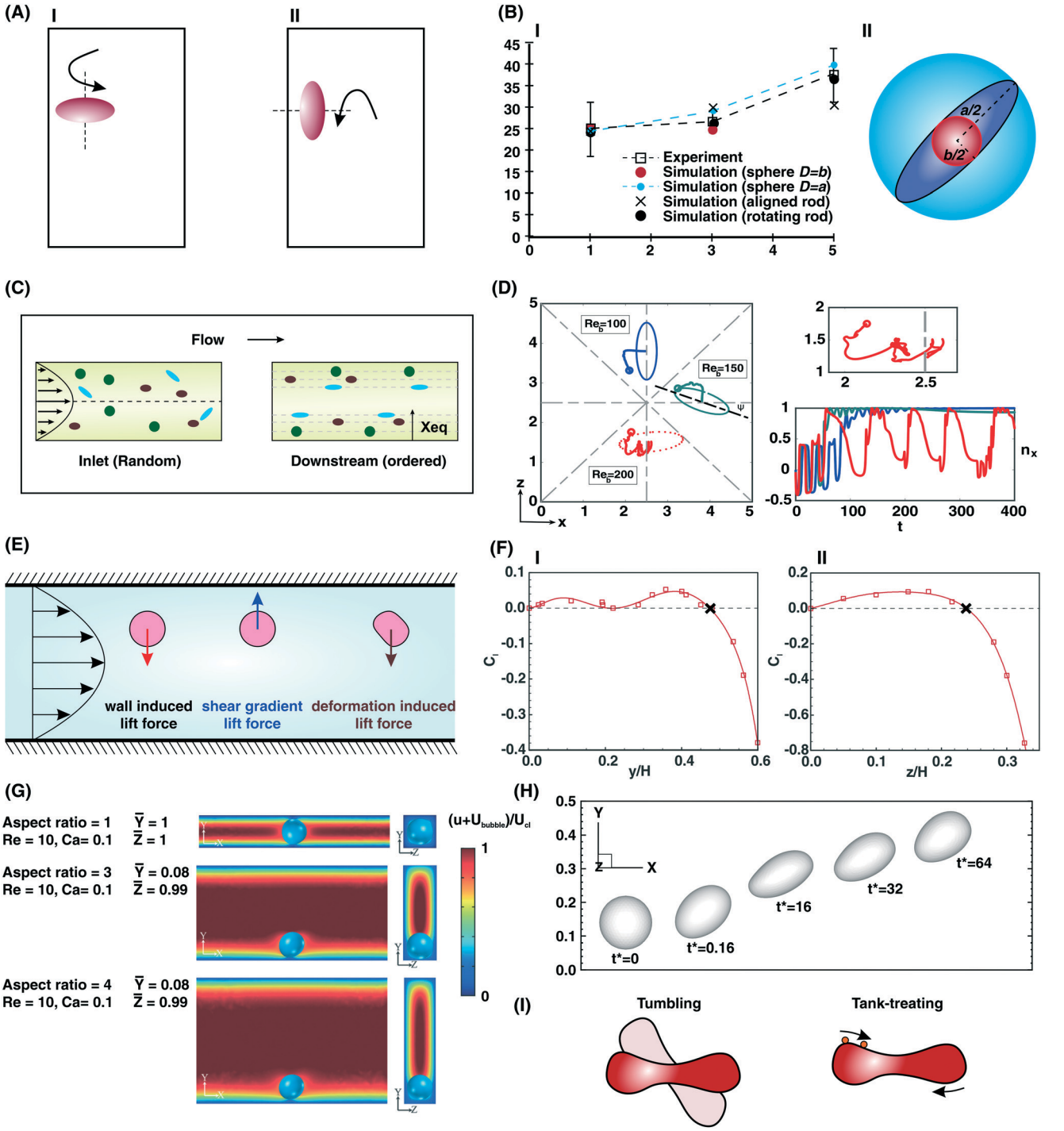

Fig. 7 Migration of non-spherical and deformable particles in confined flows. A) Components of the rotation axis of a rod-like particle in a rectangular channel; (I) in-plane rotation (II) out-of-plane rotation. B) (I) By increasing the aspect ratio of the elliptic particle, the equilibrium position moves toward the center. (II) Definition of a and b parameters. Reproduced from ref. 62 with permission under open license CC BY 3.0. C) Particles with different aspect ratios focus at distinct positions of the channel cross-section. D) The orientation of an oblate particle at the equilibrium position for different Re. At low Re (Re $<$ 100), particles stay vertical to the adjacent wall. By increasing Re to 150, particles become slightly slanted with respect to the symmetry line. Further increasing of Re causes particles to enter a tumbling motion which causes them to oscillate around a specific point (equilibrium position). Reproduced with permission from ref. 64. E) Schematic of forces acting on a deformable particle. The deformability moves particles towards the center of the channel. F) Non-dimensional lift force acting on a droplet in a rectangular channel with an aspect ratio of two. There are two different equilibrium positions (I) in the width direction (blockage ratio is 0.6) (II) height direction (blockage ratio is 0.3). Reprinted from ref. 65, with the permission of AIP Publishing. G) Equilibrium position of a bubble in rectangular channels. Reproduced from ref. 66 with permission from The Royal Society of Chemistry. H) Migration of a deformable capsule toward the center of the channel. Reprinted from ref. 67, with permission from Elsevier. I) Schematic of definitions of tumbling and tank-treat motions.

particle located at different distances from the channel cross-section center. When the particle is closest to the channel center, the weakest secondary flow is observed.

The pressure distribution across the surface of a particle plays a significant role in the lift force acting on the particle. Numerical studies show that there are four distinct regions on the surface; two minimum and two maximum pressure areas (Fig. 6F).[38,50] Since the magnitude of the pressure distribution across the areas near the channel wall is larger, the particle is repelled from the wall toward the center of the channel.

Deformable and non-spherical particles. Rigid, spherical particles are commonly used in numerical and analytical solutions of particulate flows. However, the non-spherical shape and elasticity of a particle play a vital role in the inertial particle motion. Using FSPP, Masaeli and her co-workers[62] studied the motion of rigid rod-like particles with different aspect ratios in rectangular channels. They showed that the rotation of particles is a combination of in-plane and out-of-plane rotations (Fig. 7A). By increasing Re, particles mainly exhibit in-plane rotation. Also, by increasing the aspect ratio of a particle, its equilibrium position moves toward the center of cross-section (Fig. 7B). This phenomenon has been used to separate particles with different rotational diameters[63] (Fig. 7C). Also, Lashgari *et al.*[64] investigated the migration of a single oblate particle in a duct using the IBM from moderate to high Re (Fig. 7D). To reduce the numerical calculation time, particles are released from an initial position far from the center as the particle migration velocity at the center vicinity is relatively low.

Deformability is another property of real particles (*e.g.*, cells and microgels). Deformable particle models can be divided into three categories: 1) droplet,[65,66] 2) deformable capsule,[67,68] and 3) elastic particles.[69] The deformability leads to approaching the particle equilibrium position to the channel center (Fig. 7E). When deformable particles are released in the channel, after a while, they reach a steady-state shape and migrate toward their equilibrium position. This feature of the deformable particle is due to the fact that they exhibit tank-treat motion (for periodical deformation of different points of a deformable particle see Fig. 7I) while the particle is rotating rather than tumbling, which can be observed in rigid non-spherical particles. Droplets in rectangular channels with an aspect ratio of two have two different stable equilibrium positions in a quarter of the cross-section based on the droplet size; one lies between the centerline and the wall along the width of the channel while the other one lies along the channel height (cross mark in Fig. 7F).[65] Hadikhani *et al.*[66] using the ALE method observed that by increasing the rectangular channel aspect ratio, bubbles focus at the center of the short walls, which is not similar to the behavior of rigid particles with the same size (Fig. 7G).

There are several constitutive laws for the simulation of the deformation of capsule membranes.[70,71] However, in most cases, the neo-Hookean law is used because of its compatibility with experimental results.[67] The front-tracking method,[72] as an accurate method to track the interface of a deformable object, has a formulation similar to that of IBM. However, it requires a dynamic remeshing in each iteration and thus is more time-consuming than IBM. Using a front-tracking method, Doddi and Bagchi[67] investigated the migration of deformable capsules in Poiseuille flow (Fig. 7H). Near the wall, the deformation rate is high, and after a quick deformation, the particle shape becomes approximately steady. In another study, Raffiee *et al.*[73] investigated the equilibrium position of cells with a blockage ratio of 0.2 in a square channel using the front-tracking method. According to their results, unlike rigid particles that reach equilibrium position located on the center of the channel walls, the focusing position of the cell is on the channel diagonal at the same range of Re. Villone *et al.*[69] investigated the motion of elastic spheroid particles under unbound and confined shear flows using the ALE simulation method. The results show that the wall-induced force causes more particle deformation compared to that in an unbound shear flow.

3.2.2 Inertial microfluidics in non-straight and non-planar microchannels. In the previous section, all reported studies are conducted using straight channels to investigate the physics underpinning inertial microfluidics. However, most channels used for particle manipulations are non-straight channels. In the existing numerical studies on particles' motion in these channels, the distribution of the inertial lift force in the cross-section of the channel has been calculated through the FSPP method. Then, the particle trajectories in the channel can be obtained through the point particle model by combining this force with other existing forces that have explicit formula such as drag force. These trajectories have an explicit formula[38] shown in eqn (22).

$$m_{\mathrm{p}}\frac{d^2x_{\mathrm{p}}}{dt^2} = F_{\text{Inertial force}} + F_{\text{Drag}} + F_{\text{Virtual mass}} \qquad (22)$$

Fig. 8A presents the focusing mechanism in serpentine channels.[50] In this channel, drag and inertial lift forces play a vital role in particle focusing. If the velocity of a particle exceeds a threshold, it will be focused at the center of the long walls of the serpentine channel.[74] Similar to serpentine channels, spiral microchannels have been frequently used for the separation of bio-particles and cells.[75–80] If the size of particles in spiral channels is less than a particular threshold ($a < 0.07D_{\mathrm{H}}$), the effect of the drag forces overcomes the inertial forces and traps particles in their vortex streamlines (Fig. 8B).

By changing the shape of the channel cross-section, we can control the focusing positions of the particles in a straight channel (Fig. 8C).[53,81,82] The equilibrium positions of particles can be obtained through the vector plot of the total force in any arbitrary channel cross-section by combining the calculated inertial forces from the FSPP method with the drag forces (Fig. 8D).[83] Therefore, it can be stated that particle focusing is highly related to the channel shape and cross-section, and a deep understanding of the underlying physics helps the investigator for better manipulation of the particles.

3.3. Inertial microfluidics in non-Newtonian fluids

Particles in a non-Newtonian fluid experience several lateral forces in addition to the inertial forces. The magnitude and

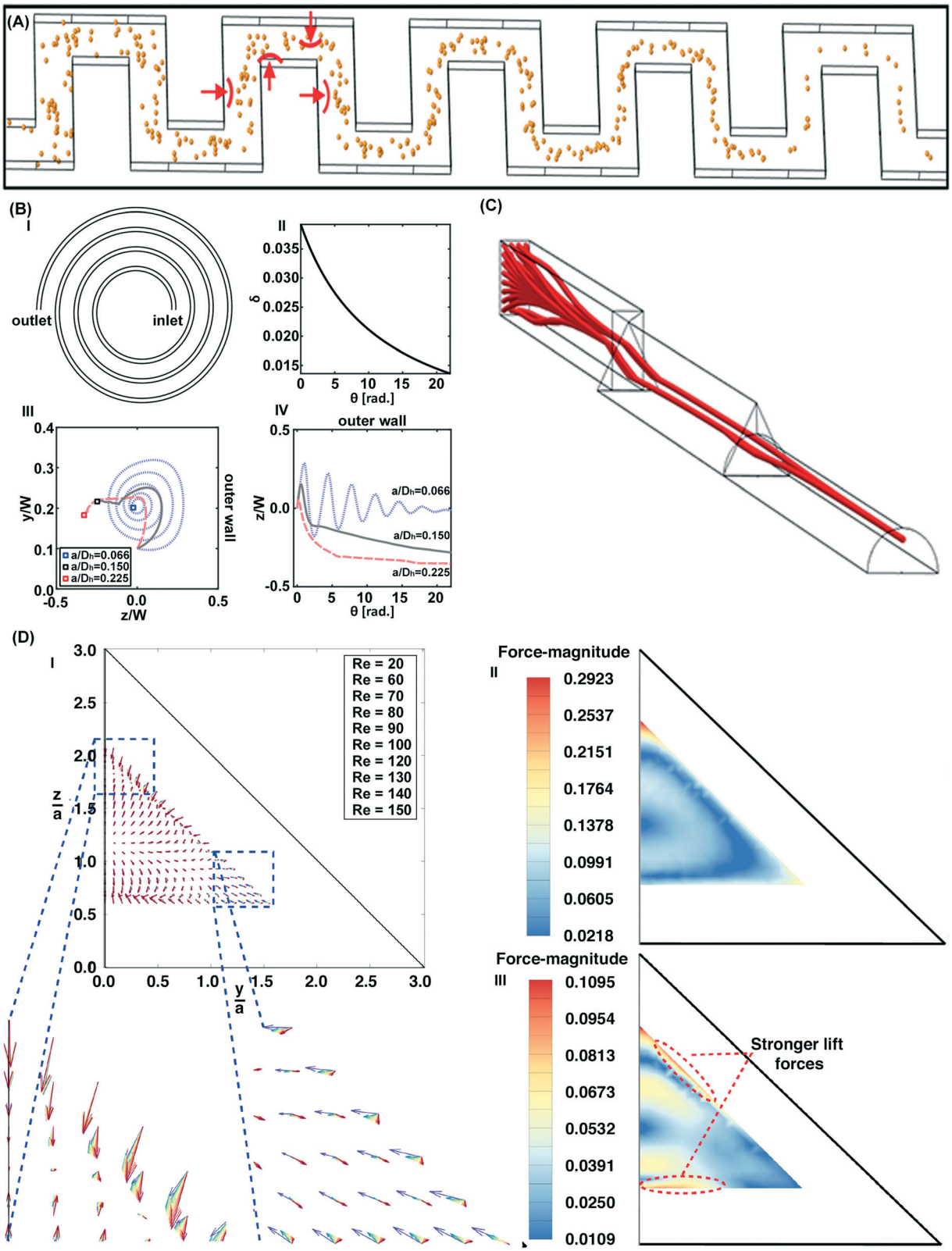

Fig. 8 Inertial microfluidics in non-straight channels. A) Particle focusing in the serpentine channel; red arrows show the direction of drag forces inside the channel. Reprinted from ref. 50 with the permission of AIP Publishing. B) I. Illustration of a spiral II. Variation of the channel curvature (δ) along the length of channel (in polar coordinates). III. The cross sectional particle trajectory for three different particles. IV. Particle migration along the length of the channel. Reprinted from ref. 77 with the permission from the Springer. C) Particle focusing in a hybrid straight channel with rectangular, triangular, and semicircular cross sections. Reprinted from ref. 53, with permission from Elsevier. D) I. Force-maps for triangular microchannel over a wide range of Re. The magnitude of lift forces for II. Re = 20 and III. Re = 150. Reproduced from ref. 83 with permission under open license CC0 1.0.

direction of these lateral forces depend on the non-Newtonian fluid's rheological properties. Therefore, the analysis of particle motion in a non-Newtonian fluid becomes more complicated compared to the Newtonian fluid. Seeing as this field is a subject of ongoing investigations, only recent major studies on particle motion in viscoelastic fluids have been reviewed.

Similar to Newtonian fluids, to obtain the flow field in a viscoelastic fluid, continuity and momentum equations need to be solved (eqn (23) and (24)). However, an extra stress tensor (τ) must be added to the total stress tensor (σ) in order to consider the effect of viscoelasticity (eqn (25)).[84]

$$\nabla \cdot u = 0 \tag{23}$$

$$\rho\left(\frac{\partial u}{\partial t} + (u\cdot\nabla)u\right) = \nabla\cdot\sigma \tag{24}$$

$$\sigma = -pI + 2\eta_s e(u) + \tau \tag{25}$$

where η_s and $e(u)$ are the Newtonian solvent viscosity and strain rate tensor, respectively. To solve this set of equations, the relation between τ and other parameters, such as fluid velocity, should be obtained by a constitutive equation.[85,86] Two constitutive laws that are frequently used are Oldroyd-B and Giesekus equation.[87] Eqn (26) shows the Giesekus constitutive law.[84] In this equation, α, η_p, and λ are the mobility factor, polymeric viscosity, and relaxation time, respectively. When the mobility factor (α) is equal to zero, the Giesekus equations is reduced to the Oldroyd-B equation.

$$\tau + \lambda\left(\frac{\delta\tau}{\delta t} + u\cdot\nabla\tau - \nabla u^T\cdot\tau - \tau\cdot\nabla u + \frac{\alpha}{\eta_p}(\tau\cdot\tau)\right) = \eta_p\left(\nabla u + \nabla u^T\right) \tag{26}$$

The migration and focusing pattern of the particles in the channel cross-section mainly depend on the competition between elastic and inertial forces acting on particles (Fig. 9A).[88–91] Li and his colleagues[92] investigated the effects of fluid elasticity, fluid inertia, and shear-thinning viscosity using Oldroyd-B (Fig. 9BI) and Giesekus equations (Fig. 9BII). They used the DLM method in the framework of the finite volume method on a staggered grid. Particles in Oldroyd-B fluid focus at the center of the channel, while in the Giesekus fluid particles reach their equilibrium at a position away from the center (Fig. 9B).

More recently, Raffiee and colleagues using the DLM method[89] studied the focusing pattern of particles in the cross-section of a square channel with Giesekus fluids for different values of Wi and Re (Fig. 9C). In another study, with a modified version of the DLM method, Yu *et al.*[90] investigated focusing patterns of particles in Oldroyd-B fluids. Fig. 9D shows the result of their study for a particle with a blockage ratio of 0.15 in a square channel under various conditions. Using FSPP, Raoufi *et al.*[88] investigated the effect of channel cross-section on focusing efficiency of elasto-inertial flows in straight channels. They have shown that by increasing the channel corner angle, the elastic force pushes the particles toward the center of the cross-section more efficiently.

To simulate the motion of cells in a square microchannel in Newtonian and viscoelastic fluid (Fig. 9E), Raffiee *et al.*[93] used the front-tracking method. The results revealed that an increase in the solution concentration led to significant enhancement in the volumetric flow rate, which can help to boost the total throughput of a microfluidic device.

4 Lattice Boltzmann method for inertial particle migration

The LBM, as an explicit alternative method for fluid dynamics problems, was introduced in 1988 by McNamara and Zanetti.[94] In this method, the fluid is approximated by discrete particle distributions moving and colliding on a regular lattice. LBM can be easily adapted for parallel processing. The numerical investigation of particle dynamics in fluids requires tracking of a solid–fluid interface where LBM is particularly powerful.[95–98] As providing the details of LBM for inertial particle microfluidics is beyond the scope of this review, please refer to textbooks, such as ref. 99 and 100.

4.1. Inertial particle motion in 2D/3D straight channels

Ladd and his team were the first to investigate inertial phenomena in microfluidic devices,[101–103] where they investigated the equilibrium positions of particles at Re of 100 to 1000 in a square duct.[104] At low Re, the numerical results were consistent with experimental ones, while at high Re, some discrepancies are raised (Fig. 10A–D). Afterward, Nakagawa and his colleagues[105] addressed this problem in their numerical study. They illustrated that for Re less than 260, the equilibrium positions were at channel faces, while for higher Re, channel corners were added to the equilibrium positions. Also, they showed an outward shift of the equilibrium positions at channel faces when Re was increased. For larger Re, the positions moved back inward (Fig. 10E–H). By combining IBM and LBM, the physical mechanism for this behavior was identified. The two vortices generated next to the particles grew upon an increase of Re, which pushes away particles from the wall.[106,107]

In a simple-shear flow profile, Mao and Alexeev evaluated particle inertia, fluid inertia, and their combination for spheroid particles with different aspect ratios at low and moderate Re.[108] The authors pointed out the possibility of superposition principle for the effects of fluid inertia and particle inertia at sufficiently low Re. They showed that Stokes number, aspect ratio, Re, and initial orientation of a single spheroid affect its trajectory. Stokes number (eqn (27)) defines the ratio of particle response time ($\tau_p = (2\rho_p + \rho_f)d_p^2/36\mu$) to fluid response time ($\tau_f = L_c/U_c$).

$$\mathrm{St} = \frac{\left(2\rho_p + \rho_f\right)d_p^{\,2}U_{max}}{36\mu D} \tag{27}$$

This number is essential for the separation of non-biological particles that are denser than water. At low Stokes numbers, particle behavior is similar to a neutrally buoyant

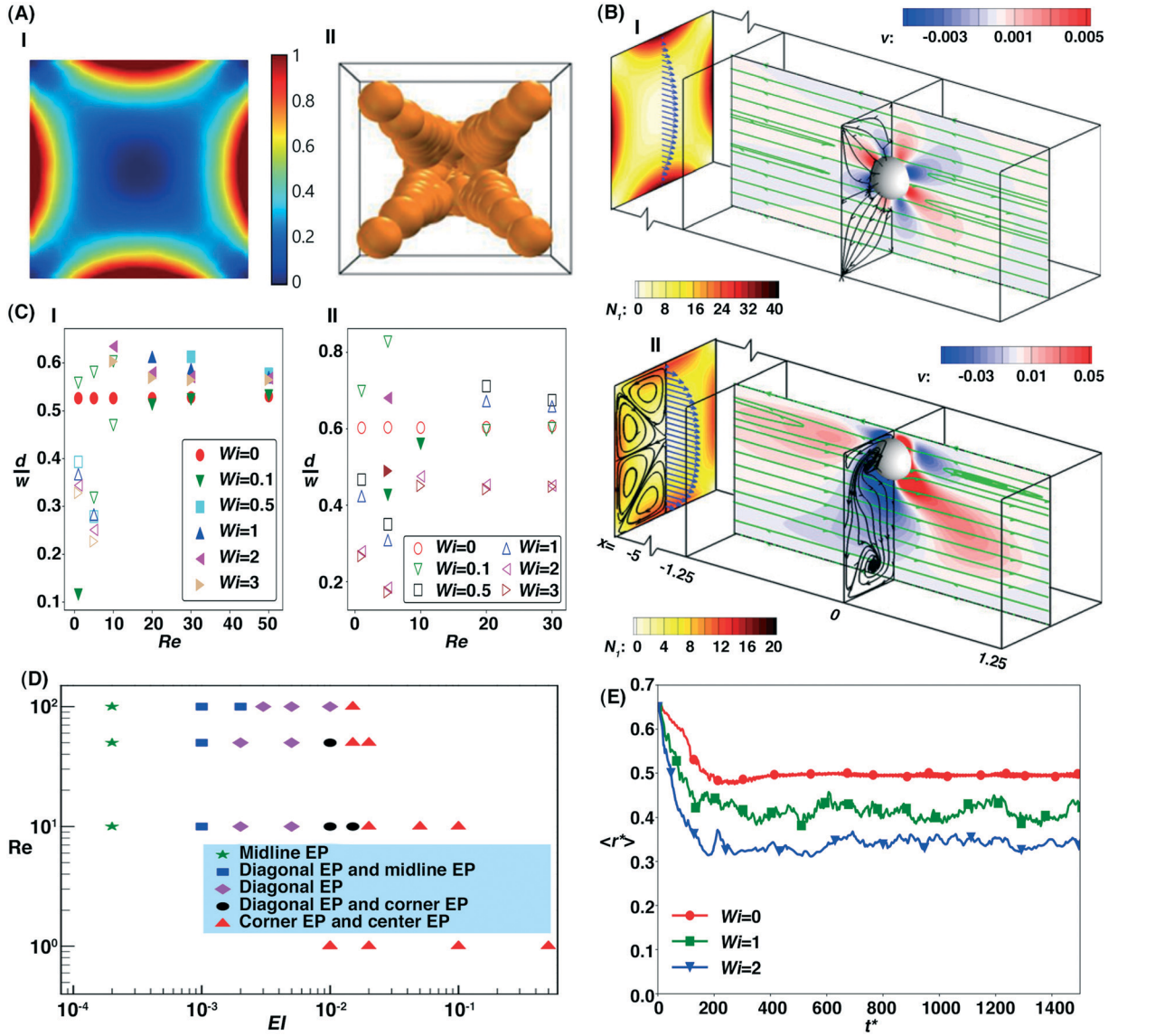

Fig. 9 A) Migration of particles in a straight channel with the viscoelastic fluid flow. I. Distribution of the shear rate in the cross-section of the channel. II. Particles move toward the minimum shear rate region. Reprinted from ref. 88, with the permission of AIP Publishing. B) Investigation of fluid behavior and particle equilibrium position in I. Oldroyd-B II. and Giesekus fluids. Reproduced with permission from ref. 92. C) the distance of the off-center lateral position of particles from the center of the channel along the I. main axis and II. diagonal of the channel for all ranges of Wi and Re. Stable equilibrium positions are identified by filled symbols, whereas unstable ones are represented by unfilled symbols. Reproduced from ref. 89 with permission under open license CC0 1.0. D) Focusing pattern of a particle with a blockage ratio of 0.15 under different conditions of El and Re. Reproduced with permission from ref. 90. E) Increasing in Wi leads to relocation of the cells toward the centerline. Reprinted from ref. 93 with the permission from the Springer.

particle,[109] while an increase in Stokes number leads to the oscillatory behavior of particles.[110]

Mao and Alexeev proposed a microchannel decorated with diagonal symmetric aligned ridges, resulting in the generation of secondary flows, for the hydrodynamic sorting of microbeads (Fig. 11A).[111] The induced secondary flows and inertial migration led to the separation of microparticles based on their sizes (Fig. 11B). However, the values of Re investigated are relatively small, and it is unclear how relevant inertial forces are. Besides ridges, wall roughness also affects the particle trajectory.[112]

With the combination of IBM, LBM, and FEM, the hydrodynamic focusing of rigid particles (r = 3, 6, and 12 μm) in a straight channel was investigated.[113] The particle trajectory (Fig. 11C) for two particles with a radius of 6 and 12 μm at Re = 83 reveals that while these two different particles show small oscillations in the interacting stage, both followed two different paths at the separation stage. Besides, particle equilibrium position (r = 6 μm) demonstrated that for high enough Re, inertial effects became dominant and pushed particles closer to the channel wall. However, an even larger Re might result in unfavorable focusing and unstable fluid dynamics (Fig. 11D). In another study, Krüger and his coworker investigated the interplay of inertial and deformability over a wide range of Re (3–417) and Ca (0.003–0.3) for the volume fraction of ϕ = 0.1.[114] They showed that for a fixed Re,

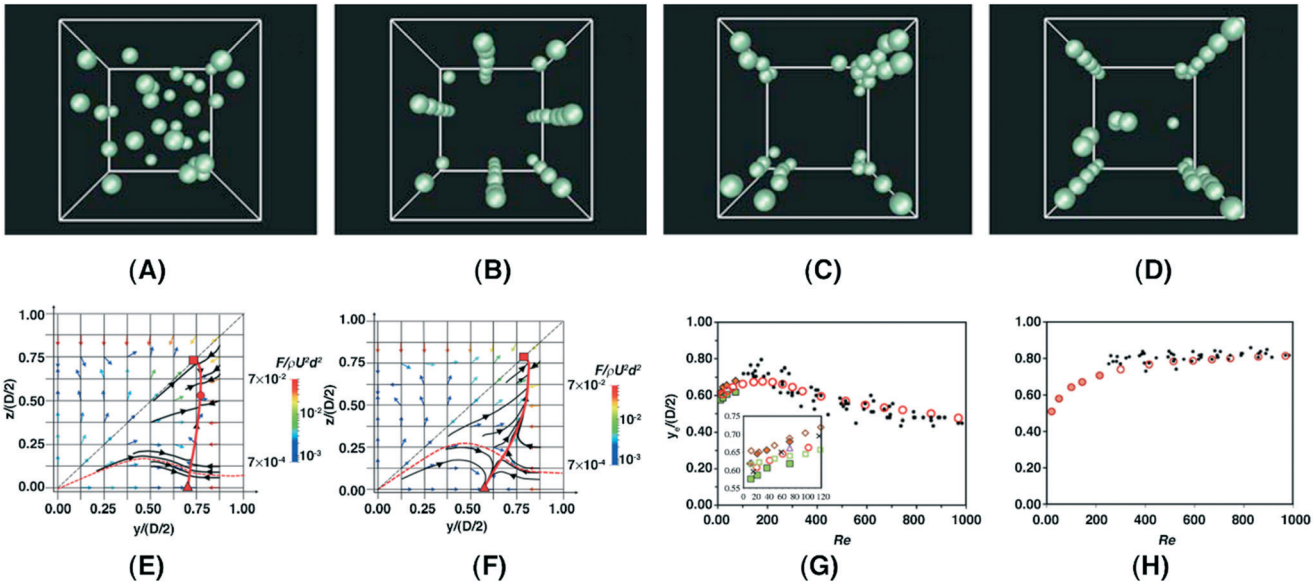

Fig. 10 A) Initial distribution of particles leads to different equilibrium positions based on Re. Particle equilibrium positions for Re of B) 100, C) 500, and D) 1000. Based on results presented by Chun and Ladd,[104] at Re = 100, particles migrated to the eight equilibrium positions. For Re = 500, particles migrated to one of four stable locations near the corner of square duct, while for Re =1000, the particle equilibrium configuration changed. Reprinted from ref. 104, with the permission of AIP Publishing. Map of lateral forces for Re of E) 260 and F) 514 calculated by Nakagawa and co-workers[105] who showed that the particle behavior and equilibrium positions change by increasing Re. Equilibrium position in G) channel face and H) channel corner. Circles are the results of their study, while experimental results are indicated by other shapes. Reproduced from ref. 105 with permission.

softer particles focused near the center-line of the microchannel (Fig. 11EI). According to their results, the higher the rigidity of the particles, the thinner the depletion layer (d), which is defined as the minimum distance of the particle surface to the wall (Fig. 11EII). For Re $>$ 45, as identified with the dotted line in Fig. 11EII, the growth of the depletion layer is significantly increased.

The entropy of particle focusing (S_p) in microfluidic devices (eqn (28)) demonstrates the connection between each particle to the cumulative performance of several particles, where probability function was identified as $p(a_s)$ and the total number of states in the system (either fluid or solid state) was recognized as n.[115] A higher ordering degree means lower focusing entropy, indicating a better focusing behavior.

$$S_p = -\sum_{S=0}^{n} p(a_s)\log p(a_s) \quad (28)$$

Focusing entropy of rigid particles was lower than soft ones (Fig. 12A), signifying better ordering behavior of rigid particles, and the rectangular cross-section showed more viability regarding hydrodynamic focusing than the square and circular ones. With the coupling of LBM and LSM, Kilimnik *et al.* investigated the migration of a deformable capsule.[116] The larger and the softer the particles are, the closer to the center they become, indicating that deformability leads to a center-facing lift force, which is a well-known effect. In addition, increasing the viscosity of the encapsulated fluid resulted in equilibrium positions closer to the wall. It has also been illustrated that in a Poiseuille flow, soft particles moved away from walls, whereas the position of hard ones is independent of the Re. Besides, the migration velocity in Poiseuille flow was 3 to 4 times higher compared to the simple shear flow due to the higher variation of velocity across the particle.[117] Prohm and Stark showed that the lateral position of particles could be manipulated by axial control forces (Fig. 12BI and BII).[118] In addition, they used the feedback control approach to apply a non-constant axial force in order to efficiently control the position of particles and increase the particle throughput (Fig. 12BIII). Based on their method, this group[119] extended their theory by investigating of deformable capsules in a microchannel by evaluating on Laplace number (Appendix 1). While deformability entirely is depended on Re, the equilibrium position approximately is independent of Re and falls into a master curve line (for each particle diameter) when plotted *versus* Laplace number. Moreover, they used external forces to control the equilibrium position of particles. Although rigid particles move away from the centerline in high Re, very soft capsules behave oppositely. Moreover, it was shown that by choosing the proper amount of flow rate, separation of a deformable capsule with different aspect ratio and membrane shear elasticity through bifurcation is achievable.[120]

The interparticle spacing in inertial microfluidics is of significant importance for such applications as imaging or flow cytometry.[121] The favored spacing in low particle Re was measured to be 5D while at high particle Re, it went to 2.5D, where D equals to particle diameter. However, an increase in concentration led to a decrease in particle spacing such that a single train of the particle could not be identified.[122] To shed more light on this matter, Liu and Wu,[123] in a 2D lattice

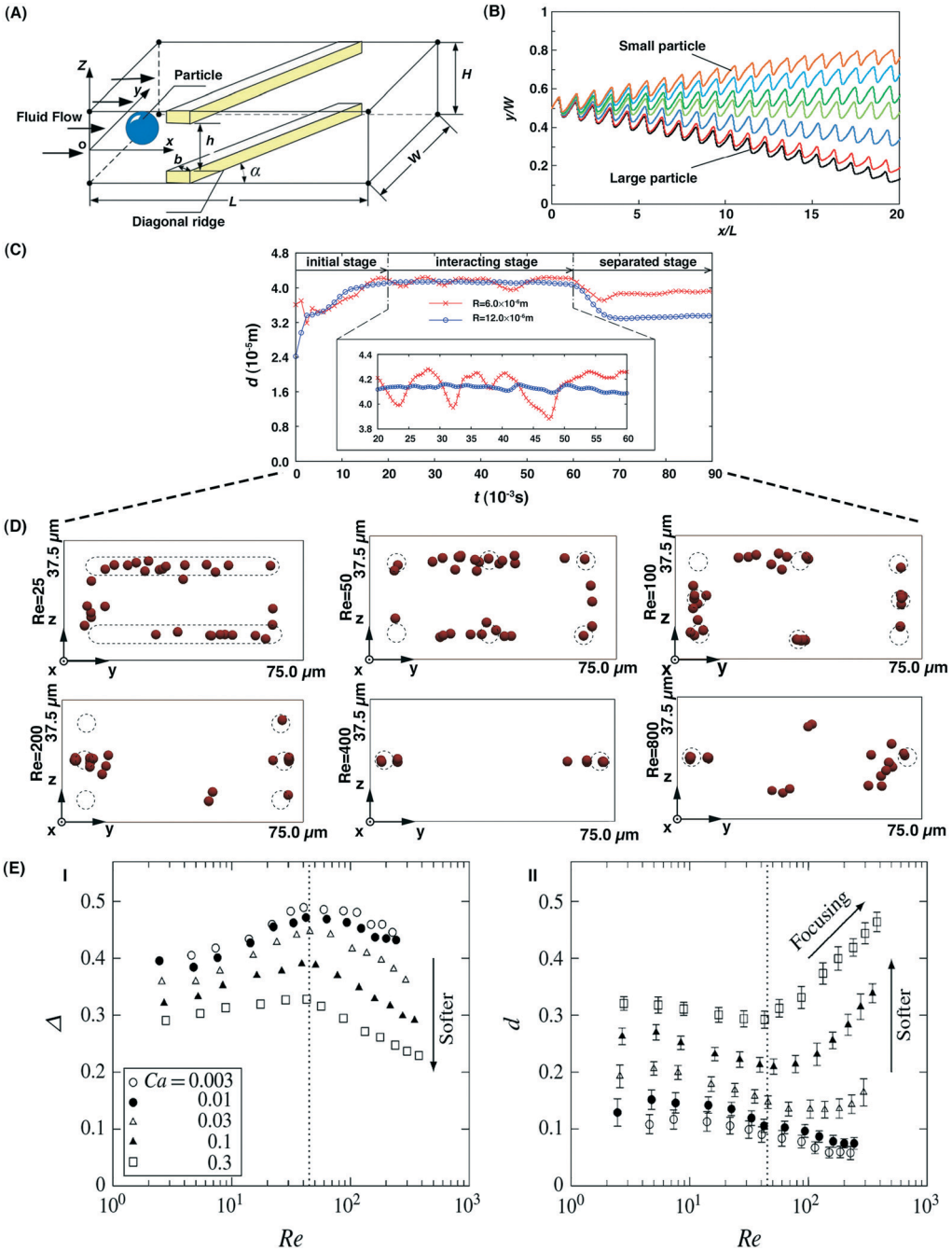

Fig. 11 A) Schematic illustration of a microfluidic device decorated with diagonal ridge developing secondary flows. B) The particle trajectory of various particles from the starting point of y/w = 0.5 was evaluated. As can be seen, the smaller particle migrated toward the positive y while larger ones migrated in the opposite direction. Different lines belong to different particles. Reprinted from ref. 111, with the permission of AIP Publishing. C) Particle trajectory for two particles with a radius of 6 and 12 μm. The whole process can be divided into three separate sections of initial, interacting, and separation stages. In the separation zone, particles with different size migrated into separate locations, indicating the ability of hydrodynamic focusing on separation of size-based microparticles. D) The transition of multiple equilibrium positions was also evaluated for particles with a radius of 6 μm. These positions in various Re are attributed to the two dominant effects of fluid shear and wall-induced forces. Dashed lines represent all possible equilibrium positions. By increasing Re, equilibrium positions relocate from the center of the longer wall to the center of the smaller wall, and it pushes particles more toward the walls. Reprinted from ref. 113, with permission from Elsevier. E) I. For a fixed value of Re, softer particles are closer to the centerline II. an increase in stiffness leads to an increase in the depletion layer. Re $>$ 45 is identified by a dotted line. Reproduced from ref. 114 with permission.

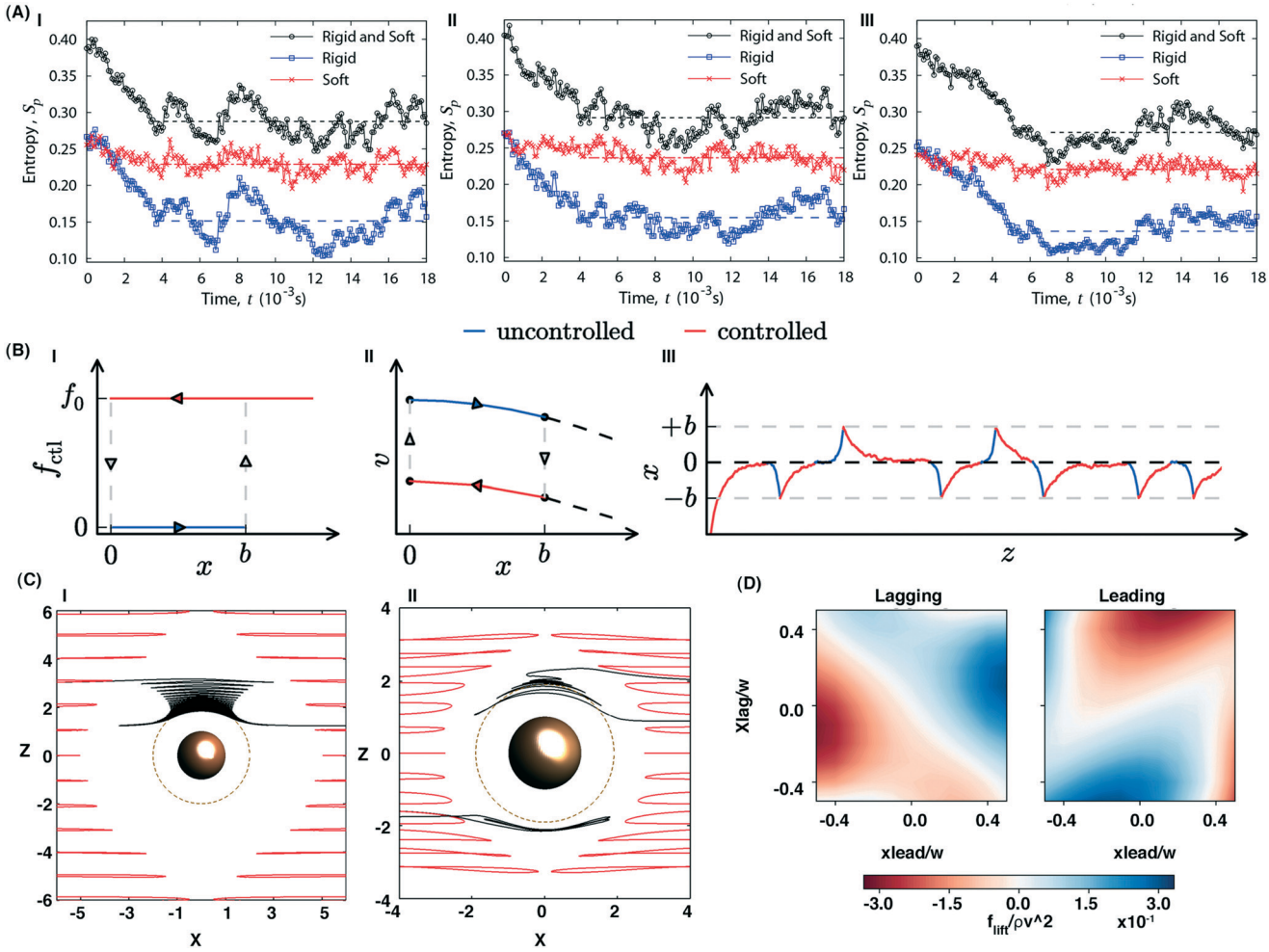

Fig. 12 A) Migration of rigid and soft particles (R = 1.5 μm) within a I. circular, II. square, and III. rectangular microchannel. The average values of entropy after initial falling were highlighted by dash lines. Reprinted from ref. 115, with permission from Elsevier. B) Schematic illustration of the feedback control. I. When the particle left the desired area (*i.e.*, [−*b*,*b*]), the axial force turned on, and it was turned off when the particle went to the centerline (*i.e.*, x = 0). II. The velocity of a particle with and without axial force control in the desired portion (*i.e.*, [−*b*,*b*] III. An example of particle trajectory in the desired interval. Reproduced from ref. 118 with permission from The Royal Society of Chemistry. C) Off-plane spiraling streamlines for an isolated pair of particles for I. Re = 0.05 and II. Re = 0.6. An increase in Re leads to decrease in the off-plane spiraling zone. Reprinted from ref. 124 with the permission of AIP Publishing D) Representation of color-coded lift profile for a pair of leading and lagging particles. Reprinted from ref. 125 with permission from the Royal Society of Chemistry.

domain, proposed a dimensionless focusing number (F_c = Re^m/ϕ^n, m = 0.36, n = 2.33) and represented that $F_c > F_c^+$ resulted in complete inertial migration while $F_c < F_c^-$ shows unfocused particles and $F_c^- < F_c < F_c^+$ led to partial particle focusing (F_c^+ and F_c^- are upper and lower limits of particle focusing, respectively). Besides the train of particles, Haddadi and Morris developed a study regarding dynamics and trajectory of isolated and suspended (solid volume fraction was less than 0.3) pair of particles.[124] They showed that pair trajectories and streamline around an isolated particle have similarities, including reversing, in-lane spiraling, off-plane spiraling (Fig. 12C), and open but fore-aft asymmetric streamlines. More recently, with more emphasis on inertial microfluidics, Schaaf and his colleagues investigated on flowing pair of particles.[125] They believed that the inertial lift profile is strongly dependent on the position of the particle in the fluid, whether it is leading or lagging (Fig. 12D). Nonetheless, by increasing the axial distance or Re, the profiles become similar to each other while having a constant shift to each other.

4.2. Inertial particle motion in non-straight microchannels

Generally, straight microchannels enjoy the features of a simple fabrication process and easy operation, and the inertial focusing mechanism is almost clear for certain specific cross-sections. However, these channels suffer from the long footprint, which impedes their further applications and makes limitations on their commercialization aspect. As an alternative, scientists set to induce secondary flows within the channel by means of obstacles, changing channel geometry, or using curved channels to assist inertial particle motion. Accordingly, the principal mechanism of particle migration becomes more intricate, requiring a robust, solid description. So far, the number of studies using LBM for the investigation

of inertial particle migration in a non-straight channel has not been significant. Due to the intricate nature of flow in curvature, it is challenging to extract the governing equations of fluid with the corresponding dominant forces acting on particles. Moreover, most of results focus on experimental studies, resulting in unclear particle–particle and particle–fluids interaction during the focusing process and unspecified particle migration in cross-section of the channel. Hence, it is anticipated that in the near future, more numerical studies focus on inertial particle migration within non-straight microchannels. In the following, we review studies conducted using LBM in a non-straight microchannel.

4.2.1 Serpentine microchannels. Serpentine microchannels have a smaller footprint compared to straight channels and bear the feature of massive parallelization. Gaining the efficiency of IB-LBM, Jiang and colleagues investigated numerically and experimentally particle focusing with a diameter of 5 and 10 μm inside a symmetrical serpentine microchannel.[126] Calculating fluid flow by LBM and particle structure by FEM, the authors integrated these two parts using IBM. In low Re, inertial lift force increased, and particles were pushed toward the sidewalls where smaller particles were closer to the walls. In high-enough Re, the dominant force turned to be drag force, Dean flow forced particles to swing out of inertial lift force trap, and particles were focused at the vicinity near the center of Dean flow vortex (Fig. 13AI and II). This focusing pattern is expressed by eqn (29) where δ is curvature ratio ($\delta = d_h/2r$, d_h is

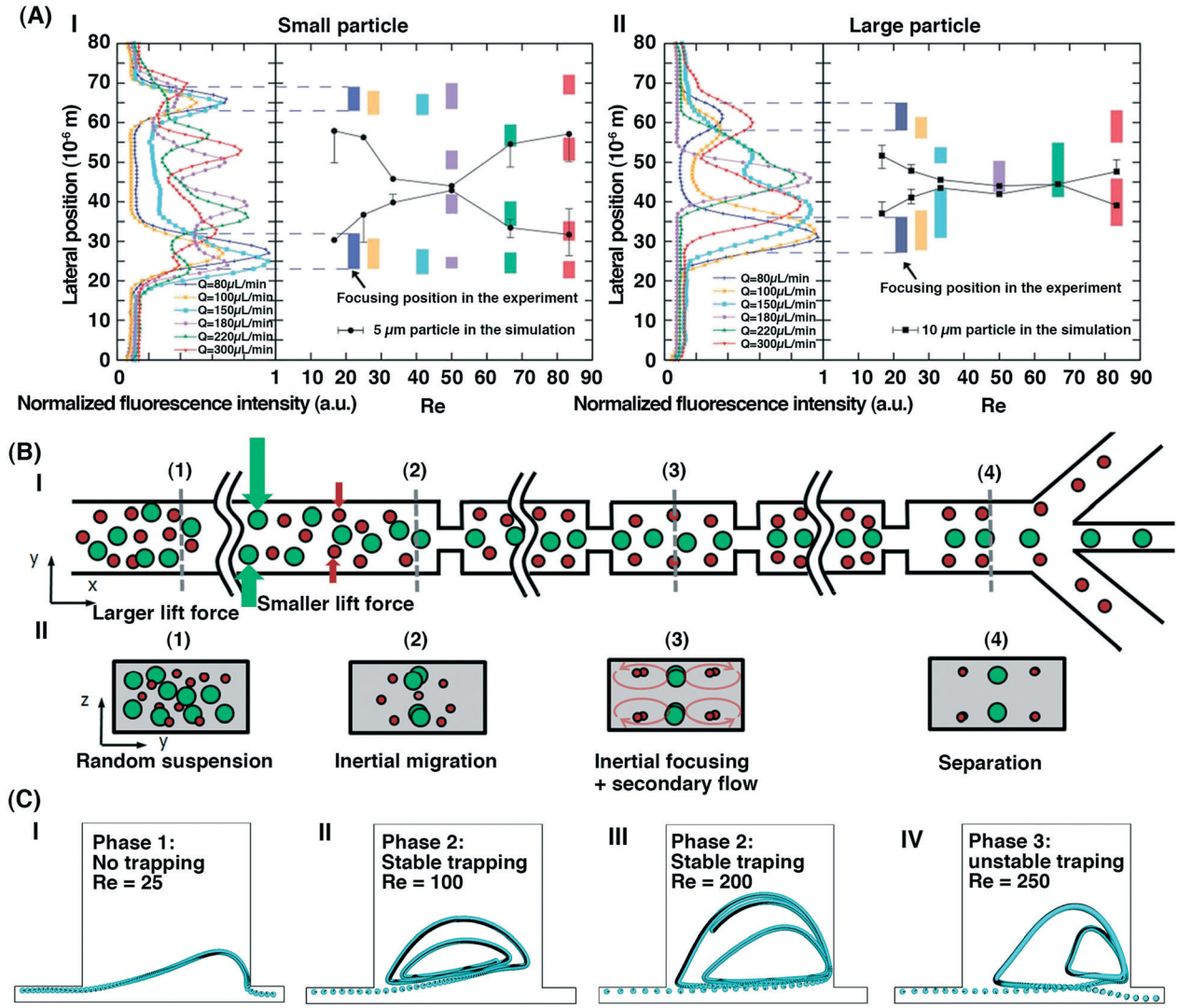

Fig. 13 A) The comparison of the lateral position of particles with different sizes in a channel. Data shown in the figure is obtained experimentally and numerically. Reproduced from ref. 126 with permission from The Royal Society of Chemistry. B) I. Schematic illustration and the design principle of the proposed contraction expansion microchannel by Wu and co-workers. II. Randomly dispersed particles were first focused due to the inertial effect. Next, at the presence of contraction-expansion arrays, secondary flows were induced resulted in the migration of small particles to the side of channel walls while maintaining large particles near the centerline of the channel. Afterward, each stream was collected from separate outlets. Reproduced from ref. 130 with permission from The Royal Society of Chemistry. C) Three particle entrapping phases I. no trapping, II. stable trapping, and III. unstable trapping. Reprinted from ref. 135 with the permission from the Springer.

hydraulic diameter and r is the channel radius) and d is particle diameter.[127,128]

$$\frac{F_L}{F_D} \sim \frac{1}{\delta}\left(\frac{d}{d_h}\right)^3 \mathrm{Re}^n, \quad (n < 0) \tag{29}$$

Based on eqn (29), an increase in Re leads to make the Dean drag force dominant.

4.2.2 Cavities and contraction–expansion arrays. Cavities, contraction–expansion arrays, and constrictions provide additional secondary flows, assisting in inertial particle migration.[129] Wu *et al.* proposed a contraction-expansion microchannel to induce additional secondary flows for particle separation (Fig. 13BI and BII).[130] They observed that particles with the diameter of 9.9 μm moved more toward the centerline than those with a diameter of 5.5 μm. However, since the concentration of the used microparticles for numerical simulation was not high enough, particle–particle, particle–wall, and particle–fluid interaction were not thoroughly investigated. Also, although contraction–expansion channels with higher expansion to contraction ratio required higher flow rates to focus size-based particles, their focusing performance is better.[131]

In another study, the vortex entrapment of particles inside a microchannel with flat and curved edges was evaluated.[132] The authors suggested that the combination of repulsive forces and inertial effects could potentially lead to liberating particles trapped in a vortex zone at high Re. It was shown later that the entrapment inside a microcavity is related to both particle dynamics and flow morphology[133] where the feasibility of these microcavities was showcased by cancer cell separation.[134] Using IB-LBM, it was revealed that the dynamics of a particle within a cavity is affected by two competitive outward centrifugal and inward inertial forces.[135] There are three particle entrapping phases: no trapping ($\mathrm{Re} < 50$, due to the lack of enough inertial forces), stable trapping ($50 \leq \mathrm{Re} \leq 200$), and unstable trapping ($\mathrm{Re} > 200$, the existence of strong fluid inertia) (Fig. 13C). Also, four trapping modes of outer to inner ($50 \leq \mathrm{Re} < 100$), invariable ($100 \leq \mathrm{Re} < 150$), inner to outer ($150 \leq \mathrm{Re} \leq 200$), and inner to escape ($\mathrm{Re} > 200$) within a microcavity occur. Within a cavity, rotating and orbiting velocity of a particle is not constant while both motions are counter-clockwise.

5 Concluding remarks and outlook

In this review, we have summarized all computational techniques for inertial microfluidic modeling and categorized them into three subsections of semi-analytical solution, direct numerical simulation, and lattice Boltzmann method. In the first, all relevant articles utilizing semi-analytical methods to simulate inertial particle focusing were reviewed. In these methods, the main important parameters are Re and confinement ratio, allowing an analytic treatment of inertia-induced migration for the calculation of lift force profiles. As these methods require the particle radius to be much smaller than the channel diameter, it is hardly applicable to microfluidic particle flow, where this assumption is often violated. Also, they cannot be implemented for coupled inertia-viscoelastic problems where complex constitutive equations exist. There are some crucial issues that need to be addressed in order to achieve more accurate and realistic solutions. The first one is overcoming the inherent complexity of solving 3D partial differential equations (PDEs) using proper analytical or semi-analytical approaches. Analytically solving a set of PDEs for the fluid (three momentum equations) coupled with a set of PDEs for particles (three linear momentum plus three angular momentum equations) and also two coupling equations at the interface of fluid and solid domains using non-homogeneous boundary conditions is nearly an impossible task. Therefore, all covered articles tried to simplify this complex problem. The second issue stems from convective terms in the momentum equations. These terms alter prior first-order PDEs to more complex second-order PDEs, implying more difficulty in solving the equations by analytical methods. Last but not least, the effect of particles on fluid flow through disturbances near the particles is another intricacy of inertial microfluidics which should be considered.

In the second section, all numerical studies on inertial particulate flows based on the Navier–Stokes equations are reviewed. These include methods such as ALE, DLM, IBM, and FSPP which are mainly used for assessing the effects of different parameters, such as particle shape, particle deformability, channel geometry, and the type of fluid on particle migration within a microchannel.

Although there has been significant progress in inertial modeling of particle motion, there are still various cases which have not been thoroughly investigated. As can be seen in Table S1,† the most uninvestigated cases are non-straight channels, non-spherical/deformable particles, and viscoelastic fluids. The reason is the complexity and time-consuming nature of these studies compared to the migration of simple rigid spherical particles in straight Newtonian fluids. The non-spherical shape of particles often requires a smaller time step, prolonging the amount of time required for numerical calculations. Moreover, among non-straight channels, those with a periodic pattern along their length (*e.g.*, serpentine or contraction–expansion arrays) can be modeled by using a single unit cell with periodic boundary conditions, rather than simulating the entire channel. Nonetheless, numerical simulations of microchannels without any periodic pattern (*e.g.*, spirals) are troublesome. Numerical simulations of viscoelastic flows in the inertial regime and fluid flow with high Wi pose some serious challenges. There is a common problem regarding the numerical convergence for fluids with high Wi dubbed the high Weissenberg number problem (HWNP). This challenge is related to the existence of steep boundary layers of conformation fields which cannot correctly be represented by low-order polynomial interpolation functions.[136] Although there are some efforts (*e.g.*, picturing the steep boundary condition using a logarithmic representation) to address this problem to some extent, this field is actively being investigated. The need for further investigation is more evident when one considers a combination of the above-

mentioned conditions, namely deformable and non-spherical particles in non-straight channels in viscoelastic fluids.

It would be significant to assess the capability of existing commercial CFD packages for simulation of inertial microfluidics and give an insight to those who want to use them for their studies. There exist various commercial CFD software such as COMSOL Multiphysics, ANSYS Fluent, OpenFOAM, or Flow-3D. Using these software packages dramatically reduces the efforts required to write bespoke CFD codes. Nevertheless, using these packages for the simulation of particle motion in inertial and viscoelastic flows brings about several problems. Most of these packages can deal with particle motion, such as the particle tracing module in COMSOL. As mentioned earlier, these modules treat particles as point particles, indicating that forces acting on particles are calculated through a series of equations (*e.g.*, Stokes drag). The problem with this approach is that the exact formula for the inertial forces acting on the particle in terms of flow parameters and particle properties is unknown. Although COMSOL, as a pioneer in this field, provides an approximate formula for inertial forces, the numerical model in some cases gives incorrect and inaccurate results for 3D flows. Therefore, it is necessary to calculate the interaction between the finite-size particles and the fluid. This requires fluid–structure interaction (FSI) which is in principle available in most commercial software packages. However, since current FSI modules do not have periodic boundary condition for moving particles at the inlet and outlet of channel unit cell, they cannot be implemented to the particle motion simulation. For simulating viscoelastic fluids, it is appropriate to use constitutive equations such as Giesekus or Oldroyd-B that are consistent with experimental results; but these models are not defined by default in current software packages. Altogether, it is not possible or practical to accurately simulate particle motion in inertial and viscoelastic flows using commercial software packages in their default mode, and additional scripts must be written. Using these scripts, it is possible to use periodic boundary conditions in a part of the domain or to add constitutive equations for viscoelastic fluids to commercial packages.

In the third section, all numerical studies based on LBM were reviewed. Initially, numerical results obtained using LBM were not entirely in line with those obtained from experiments. More recent results, however, illustrate that LBM can now accurately predict the particle behavior in inertial microfluidics. LBM has a strong potential to be applied to inertial microfluidics and can be considered as a robust, efficient, and powerful alternative to conventional Navier–Stokes solvers in many fluid flow problems.

LBM is mostly limited to viscous fluids, and more research is needed to extend the method to viscoelastic fluids. Since the LBM in its original form depends on a cubic lattice, it is challenging to apply the method to geometries such as spirals due to the large "dead" volume. This explains why the LBM has mostly been used to study inertial flows in straight channels. Sparse geometry LBM codes can be applied to geometries such as spirals more easily, and more development work in this field is needed. Due to the large number of different lattice Boltzmann boundary condition schemes available for moving and stationary objects, it is yet to be decided which methods are most suitable and reliable for inertial particle microfluidic applications. Since the LBM is a weakly compressible scheme, it is not very accurate for the pressure field, which may negatively affect the lift and drag forces acting on moving particles. Although recent LBM studies have shown considerable progress in enhanced computational performance, non-spherical particles (using DSP-LBM method), or non-Newtonian fluids,[137–140] more research is needed to investigate the accuracy and reliability of the LBM for inertial particle microfluidics.

In conclusion, computational inertial microfluidics is a nascent field, requiring more devoted studies to develop and describe the underlying physics. Please refer to Table S1 in ESI† for the current contribution of computational methods in inertial microfluidics. Most of the studies published so far are not comprehensive since the developed codes and models are limited to specific channel geometries or particle properties, mostly rectangular straight microchannels and rigid spherical particles. New computational packages, commercial and scientific, need to be developed that can predict the migration of realistic particles in complex flow geometries, depending on initial conditions, flow parameters, and particle concentration.

Appendix 1

Dimensionless parameters in inertial microfluidics

Reynolds number (Re). Re is one of the most important dimensionless numbers in fluid mechanics, representing fluid behavior in various situations. Re is the ratio of inertial to viscous effects, as shown in eqn (S1). In this text, we refer to channel Reynolds number as Re. Here, ρ is the fluid density, μ is the fluid dynamic viscosity, u is the mean velocity of the fluid, and D_h is the hydraulic diameter of the channel.

$$\mathrm{Re} = \frac{\rho u D_h}{\mu} \tag{S1}$$

Particle Reynolds number ($\mathrm{Re_p}$).

$$\mathrm{Re_p} = \mathrm{Re}\left(\frac{a}{H}\right)^2 \tag{S2}$$

where a is particle diameter and H is channel dimension.

Blockage ratio (κ). The blockage ratio is defined as the ratio between particle diameter to the characteristic length of channel (height of the channel cross-section). If the blockage ratio is more than 1, the channel gets blocked.

$$\kappa = \frac{a}{H} \tag{S3}$$

Dean number (De). This number characterizes the strength of secondary flows generated in a curved

microchannel, which relies on Re, the hydraulic diameter of the channel (D_h), and the radius of channel curvature (R).

$$De = Re\sqrt{\frac{D_h}{2R}} \quad (S4)$$

Capillary number (Ca). For a droplet with surface tension σ, capillary number is defined as the ratio of viscous stress to surface tension.[141]

$$Ca_{droplet} = \frac{\mu_{ex} U_{max} a}{\sigma W} \quad (S5)$$

where μ_{ex} is the dynamic viscosity of the continuous phase fluid, U_{max} is the maximum velocity, and W is the channel width. For a deformable capsule or elastic particle, Ca is considered as the ratio between the viscous force and elastic force, while the elastic modulus takes different forms depends on capsules or bulk elastic particles.[67,142]

Laplace number (La). Ca for a deformable capsule depends on the flow characteristics (*i.e.*, flow speed). La is a dimensionless number that characterizes the rigidity of a capsule based on the elastic shear force ($\kappa_s a$, κ_s is shear modulus) and intrinsic inertial force scale (ρv^2), without depending on the explicit flow speed.[119] Using Re_p, La can be written as eqn (S6).

$$La = \frac{\kappa_s a}{\rho v^2} \quad (S6)$$

Weissenberg number (Wi). Wi relates the intrinsic time scale of a relaxation process (*e.g.*, polymer shape recovery) and the time scale of a shear flow. For large Wi, the deformable object has not enough time to relax. Here, λ is relaxation time and $\dot{\gamma}$ is the shear rate.

$$Wi = \lambda\dot{\gamma} \quad (S7)$$

Elasticity number (EI). EI characterizes the behavior of a viscoelastic fluid; it is the ratio between Wi and Re.

$$El = \frac{Wi}{Re} \quad (S8)$$

Conflicts of interest

There are no conflicts to declare.

Acknowledgements

M. E. W. would like to acknowledge the support of the Australian Research Council through Discovery Project Grants (DP170103704 and DP180103003) and the National Health and Medical Research Council through the Career Development Fellowship (APP1143377).

References

1 G. M. Whitesides, The origins and the future of microfluidics, *Nature*, 2006, **442**(7101), 368–373, DOI: 10.1038/nature05058.
2 C. Lifesciences, B. Coulter, A. Biosciences, B. Nanosciences, P. Elmer and B. Biosciences, Microfluidics in commercial applications; an industry perspective, *Lab Chip*, 2006, **6**, 1118–1121.
3 A. A. S. Bhagat, H. Bow, H. W. Hou, S. J. Tan, J. Han and C. T. Lim, Microfluidics for cell separation, *Med. Biol. Eng. Comput.*, 2010, **48**(10), 999–1014.
4 P. Sajeesh and A. K. Sen, Particle separation and sorting in microfluidic devices: a review, *Microfluid. Nanofluid.*, 2014, **17**(1), 1–52.
5 T. Salafi, K. K. Zeming and Y. Zhang, Advancements in microfluidics for nanoparticle separation, *Lab Chip*, 2017, **17**(1), 11–33, DOI: 10.1039/C6LC01045H.
6 C. Wyatt Shields Iv, C. D. Reyes and G. P. López, Microfluidic cell sorting: a review of the advances in the separation of cells from debulking to rare cell isolation, *Lab Chip*, 2015, **15**(5), 1230–1249, DOI: 10.1039/C4LC01246A.
7 Y. Gou, Y. Jia, P. Wang and C. Sun, Progress of inertial microfluidics in principle and application, *Sensors*, 2018, **18**(6), 1762.
8 D. Stoecklein and D. Di Carlo, Nonlinear microfluidics, *Anal. Chem.*, 2018, **91**(1), 296–314.
9 J. Zhang, *et al.*, Fundamentals and applications of inertial microfluidics: a review, *Lab Chip*, 2016, **16**(1), 10–34.
10 D. Di Carlo, Inertial microfluidics, *Lab Chip*, 2009, **9**(21), 3038–3046.
11 T. Zhang, *et al.*, Focusing of sub-micrometer particles in microfluidic devices, *Lab Chip*, 2020, **20**(1), 35–53.
12 D. Yuan, *et al.*, Recent progress of particle migration in viscoelastic fluids, *Lab Chip*, 2018, **18**(4), 551–567.
13 G. Segre and A. Silberberg, Radial particle displacements in Poiseuille flow of suspensions, *Nature*, 1961, **189**(4760), 209.
14 G. Segré and A. Silberberg, Behaviour of macroscopic rigid spheres in Poiseuille flow: Part 1. Determination of local concentration by statistical analysis of particle passages through crossed light beams, *J. Fluid Mech.*, 1962, **14**(1), 115–135.
15 G. Segré and A. Silberberg, Behaviour of macroscopic rigid spheres in Poiseuille flow: Part 2. Experimental results and interpretation, *J. Fluid Mech.*, 1962, **14**(1), 136–157.
16 H. Brenner, The slow motion of a sphere through a viscous fluid towards a plane surface, *Chem. Eng. Sci.*, 1961, **16**(3–4), 242–251.
17 S. I. Rubinow and J. B. Keller, The transverse force on a spinning sphere moving in a viscous fluid, *J. Fluid Mech.*, 1961, **11**(3), 447–459.
18 G. Segré and A. Silberberg, Radial particle displacements in poiseuille flow of suspensions, *Nature*, 1961, **189**(4760), 209–210.
19 P. G. Saffman, The lift on a small sphere in a slow shear flow, *J. Fluid Mech.*, 1965, **22**(2), 385–400.
20 C. K. W. Tam and W. A. Hyman, Transverse motion of an elastic sphere in a shear field, *J. Fluid Mech.*, 1973, **59**(01), 177.
21 B. P. Ho and L. G. Leal, Inertial migration of rigid spheres in two-dimensional unidirectional flows, *J. Fluid Mech.*, 1974, **65**(2), 365–400.

22 B. P. Ho and L. G. Leal, Migration of rigid spheres in a two-dimensional unidirectional shear flow of a second-order fluid, *J. Fluid Mech.*, 1976, **76**(4), 783–799.
23 J. A. Schonberg and E. J. Hinch, Inertial migration of a sphere in Poiseuille flow, *J. Fluid Mech.*, 1989, **203**(517), 517–524.
24 E. S. Asmolov, The inertial lift on a spherical particle in a plane poiseuille flow at large channel Reynolds number, *J. Fluid Mech.*, 1999, **381**, 63–87.
25 J. P. Matas, J. F. Morris and É. Guazzelli, Lateral force on a rigid sphere in large-inertia laminar pipe flow, *J. Fluid Mech.*, 2009, **621**, 59–67.
26 J. P. Matas, J. F. Morris and É. Guazzelli, Inertial migration of rigid spherical particles in Poiseuille flow, *J. Fluid Mech.*, 2004, **515**, 171–195.
27 K. Hood, S. Lee and M. Roper, Inertial migration of a rigid sphere in three-dimensional Poiseuille flow, *J. Fluid Mech.*, 2015, **765**, 452–479.
28 E. S. Asmolov, A. L. Dubov, T. V. Nizkaya, J. Harting and O. I. Vinogradova, Inertial focusing of finite-size particles in microchannels, *J. Fluid Mech.*, 2018, **840**, 613–630.
29 S. Rubinow and J. B. Keller, The transverse force on a spinning sphere moving in a viscous fluid, *J. Fluid Mech.*, 1961, **11**(3), 447–459.
30 P. Saffman, The lift on a small sphere in a slow shear flow, *J. Fluid Mech.*, 1965, **22**(2), 385–400.
31 T. Auton, The lift force on a spherical body in a rotational flow, *J. Fluid Mech.*, 1987, **183**, 199–218.
32 R. Cox and H. Brenner, The lateral migration of solid particles in Poiseuille flow—I Theory, *Chem. Eng. Sci.*, 1968, **23**(2), 147–173.
33 B. Ho and L. Leal, Inertial migration of rigid spheres in two-dimensional unidirectional flows, *J. Fluid Mech.*, 1974, **65**(2), 365–400.
34 R. Cox and S. Hsu, The lateral migration of solid particles in a laminar flow near a plane, *Int. J. Multiphase Flow*, 1977, **3**(3), 201–222.
35 P. Vasseur and R. Cox, The lateral migration of a spherical particle in two-dimensional shear flows, *J. Fluid Mech.*, 1976, **78**(2), 385–413.
36 J. Feng, H. H. Hu and D. D. Joseph, Direct simulation of initial value problems for the motion of solid bodies in a Newtonian fluid Part 1. Sedimentation, *J. Fluid Mech.*, 1994, **261**, 95–134.
37 X. Shao, Z. Yu and B. Sun, Inertial migration of spherical particles in circular Poiseuille flow at moderately high Reynolds numbers, *Phys. Fluids*, 2008, **20**(10), 103307.
38 C. Liu, G. Hu, X. Jiang and J. Sun, Inertial focusing of spherical particles in rectangular microchannels over a wide range of Reynolds numbers, *Lab Chip*, 2015, **15**(4), 1168–1177, DOI: 10.1039/C4LC01216J.
39 B. H. Yang, J. Wang, D. D. Joseph, H. H. Hu, T.-W. Pan and R. Glowinski, Migration of a sphere in tube flow, *J. Fluid Mech.*, 2005, **540**, 109–131.
40 D. Di Carlo, J. F. Edd, K. J. Humphry, H. A. Stone and M. Toner, Particle Segregation and Dynamics in Confined Flows, *Phys. Rev. Lett.*, 2009, **102**(9), 094503.
41 T. J. R. Hughes, W. K. Liu and T. K. Zimmermann, Lagrangian-Eulerian finite element formulation for incompressible viscous flows, *Comput. Methods Appl. Mech. Eng.*, 1981, **29**(3), 329–349.
42 H. H. Hu, D. D. Joseph and M. J. Crochet, Direct simulation of fluid particle motions, *Theor. Comput. Fluid Dyn.*, 1992, **3**(5), 285–306.
43 A. Prosperetti and G. Tryggvason, *Computational methods for multiphase flow*, Cambridge University Press, 2009.
44 R. Glowinski, T. W. Pan, T. I. Hesla and D. D. Joseph, A distributed Lagrange multiplier/fictitious domain method for particulate flows, *Int. J. Multiphase Flow*, 1999, **25**(5), 755–794.
45 C. S. Peskin, The immersed boundary method, *Acta Numer.*, 2003, **11**, 479–517.
46 R. Mittal and G. Iaccarino, Immersed boundary methods, *Annu. Rev. Fluid Mech.*, 2005, **37**(1), 239–261.
47 M. Uhlmann, An immersed boundary method with direct forcing for the simulation of particulate flows, *J. Comput. Phys.*, 2005, **209**(2), 448–476.
48 W.-P. Breugem, A second-order accurate immersed boundary method for fully resolved simulations of particle-laden flows, *J. Comput. Phys.*, 2012, **231**(13), 4469–4498.
49 S. Xu, F. Xu, A. Kommajosula, M.-C. Hsu and B. Ganapathysubramanian, Immersogeometric analysis of moving objects in incompressible flows, *Comput. Fluids*, 2019, **189**, 24–33.
50 A. Shamloo and A. Mashhadian, Inertial particle focusing in serpentine channels on a centrifugal platform, *Phys. Fluids*, 2018, **30**(1), 012002.
51 N. Patankar, P. Huang, T. Ko and D. Joseph, Lift-off of a single particle in Newtonian and viscoelastic fluids by direct numerical simulation, *J. Fluid Mech.*, 2001, **438**, 67–100.
52 D. Joseph and D. Ocando, Slip velocity and lift, *J. Fluid Mech.*, 2002, **454**, 263–286.
53 A. Mashhadian and A. Shamloo, Inertial microfluidics: A method for fast prediction of focusing pattern of particles in the cross section of the channel, *Anal. Chim. Acta*, 2019, **1083**, 137–149.
54 A. A. S. Bhagat, S. S. Kuntaegowdanahalli and I. Papautsky, Inertial microfluidics for continuous particle filtration and extraction, *Microfluid. Nanofluid.*, 2009, **7**(2), 217–226.
55 A. A. S. Bhagat, S. S. Kuntaegowdanahalli and I. Papautsky, Enhanced particle filtration in straight microchannels using shear-modulated inertial migration, *Phys. Fluids*, 2008, **20**(10), 101702.
56 H. Udono and M. Sakai, A numerical study on dynamic inertial focusing of microparticles in a confined flow, *Granular Matter*, 2017, **19**(4), 79.
57 Q. Wang, D. Yuan and W. Li, Analysis of Hydrodynamic Mechanism on Particles Focusing in Micro-Channel Flows, *Micromachines*, 2017, **8**(7), 197.

58 R. K. Singh and K. Sarkar, Inertial effects on the dynamics, streamline topology and interfacial stresses due to a drop in shear, *J. Fluid Mech.*, 2011, **683**, 149–171.
59 W. Lee, H. Amini, H. A. Stone and D. Di Carlo, Dynamic self-assembly and control of microfluidic particle crystals, *Proc. Natl. Acad. Sci. U. S. A.*, 2010, **107**(52), 22413–22418.
60 H. Amini, E. Sollier, W. M. Weaver and D. Di Carlo, Intrinsic particle-induced lateral transport in microchannels, *Proc. Natl. Acad. Sci. U. S. A.*, 2012, **109**(29), 11593–11598.
61 D. R. Mikulencak and J. F. Morris, Stationary shear flow around fixed and free bodies at finite Reynolds number, *J. Fluid Mech.*, 2004, **520**, 215–242.
62 M. Masaeli, *et al.*, Continuous inertial focusing and separation of particles by shape, *Phys. Rev. X*, 2012, **2**(3), 031017.
63 E. Sollier, *et al.*, *Effect of particle shape on inertial focusing*, 2011.
64 I. Lashgari, M. N. Ardekani, I. Banerjee, A. Russom and L. Brandt, Inertial migration of spherical and oblate particles in straight ducts, *J. Fluid Mech.*, 2017, **819**, 540–561.
65 X. Chen, C. Xue, L. Zhang, G. Hu, X. Jiang and J. Sun, Inertial migration of deformable droplets in a microchannel, *Phys. Fluids*, 2014, **26**(11), 112003.
66 P. Hadikhani, *et al.*, Inertial manipulation of bubbles in rectangular microfluidic channels, *Lab Chip*, 2018, **18**(7), 1035–1046.
67 S. K. Doddi and P. Bagchi, Lateral migration of a capsule in a plane Poiseuille flow in a channel, *Int. J. Multiphase Flow*, 2008, **34**(10), 966–986.
68 S. J. Shin and H. J. Sung, Inertial migration of an elastic capsule in a Poiseuille flow, *Phys. Rev. E: Stat., Nonlinear, Soft Matter Phys.*, 2011, **83**(4), 046321.
69 M. M. Villone, G. D'Avino, M. A. Hulsen and P. L. Maffettone, Dynamics of prolate spheroidal elastic particles in confined shear flow, *Phys. Rev. E: Stat., Nonlinear, Soft Matter Phys.*, 2015, **92**(6), 062303.
70 D. BarthÈS-Biesel, A. Diaz and E. Dhenin, Effect of constitutive laws for two-dimensional membranes on flow-induced capsule deformation, *J. Fluid Mech.*, 2002, **460**, 211–222.
71 E. Lac, D. BarthÈS-Biesel, N. A. Pelekasis and J. Tsamopoulos, Spherical capsules in three-dimensional unbounded Stokes flows: effect of the membrane constitutive law and onset of buckling, *J. Fluid Mech.*, 2004, **516**, 303–334.
72 S. O. Unverdi and G. Tryggvason, A front-tracking method for viscous, incompressible, multi-fluid flows, *J. Comput. Phys.*, 1992, **100**(1), 25–37.
73 A. H. Raffiee, S. Dabiri and A. M. Ardekani, Elasto-inertial migration of deformable capsules in a microchannel, *Biomicrofluidics*, 2017, **11**(6), 064113.
74 C. Liu, C. Xue, J. Sun and G. Hu, A generalized formula for inertial lift on a sphere in microchannels, *Lab Chip*, 2016, **16**(5), 884–892.
75 S. Ghadami, R. Kowsari-Esfahan, M. S. Saidi and K. Firoozbakhsh, Spiral microchannel with stair-like cross section for size-based particle separation, *Microfluid. Nanofluid.*, 2017, **21**(7), 115.
76 R. Rasooli and B. Çetin, Assessment of Lagrangian Modeling of Particle Motion in a Spiral Microchannel for Inertial Microfluidics, *Micromachines*, 2018, **9**(9), 433.
77 M. Garcia and S. Pennathur, A model for inertial particles in curvilinear flows, *Microfluid. Nanofluid.*, 2019, **23**(5), 63.
78 A. S. Rzhevskiy, *et al.*, Rapid and Label-Free Isolation of Tumour Cells from the Urine of Patients with Localised Prostate Cancer Using Inertial Microfluidics, *Cancers*, 2019, **12**(1), 81.
79 M. R. Condina, B. A. Dilmetz, S. Razavi Bazaz, J. Meneses, M. Ebrahimi Warkiani and P. Hoffmann, Rapid separation and identification of beer spoilage bacteria by inertial microfluidics and MALDI-TOF mass spectrometry, *Lab Chip*, 2019, **19**(11), 1961–1970, DOI: 10.1039/C9LC00152B.
80 T. Kwon, *et al.*, Microfluidic cell retention device for perfusion of mammalian suspension culture, *Sci. Rep.*, 2017, **7**(1), 6703.
81 J. Kim, J. Lee, C. Wu, S. Nam, D. Di Carlo and W. Lee, Inertial focusing in non-rectangular cross-section microchannels and manipulation of accessible focusing positions, *Lab Chip*, 2016, **16**(6), 992–1001.
82 J.-a. Kim, J.-R. Lee, T.-J. Je, E.-c. Jeon and W. Lee, Size-Dependent Inertial Focusing Position Shift and Particle Separations in Triangular Microchannels, *Anal. Chem.*, 2018, **90**(3), 1827–1835.
83 A. Kommajosula, J.-a. Kim, W. Lee and B. Ganapathysubramanian, High throughput, automated prediction of focusing patterns for inertial microfluidics, 2019, arXiv preprint arXiv:1901.05561.
84 A. N. Beris, M. Avgousti and A. Souvaliotis, Spectral calculations of viscoelastic flows: evaluation of the Giesekus constitutive equation in model flow problems, *J. Non-Newtonian Fluid Mech.*, 1992, **44**, 197–228.
85 R. G. Larson, *Constitutive Equations for Polymer Melts and Solutions: Butterworths Series in Chemical Engineering*, Butterworth-Heinemann, 2013.
86 R. Keunings, Finite element methods for integral viscoelastic fluids, *Rheol. Rev.*, 2003, 167–196.
87 G. D'Avino and P. L. Maffettone, Particle dynamics in viscoelastic liquids, *J. Non-Newtonian Fluid Mech.*, 2015, **215**, 80–104.
88 M. A. Raoufi, A. Mashhadian, H. Niazmand, M. Asadnia, A. Razmjou and M. E. Warkiani, Experimental and numerical study of elasto-inertial focusing in straight channels, *Biomicrofluidics*, 2019, **13**(3), 034103.
89 A. H. Raffiee, A. M. Ardekani and S. Dabiri, Particle focusing pattern in viscoelastic microfluidic devices, 2019, arXiv preprint arXiv:1904.05397.
90 Z. Yu, P. Wang, J. Lin and H. H. Hu, Equilibrium positions of the elasto-inertial particle migration in rectangular channel flow of Oldroyd-B viscoelastic fluids, *J. Fluid Mech.*, 2019, **868**, 316–340.
91 M. Trofa, M. Vocciante, G. D'Avino, M. A. Hulsen, F. Greco and P. L. Maffettone, Numerical simulations of the

competition between the effects of inertia and viscoelasticity on particle migration in Poiseuille flow, *Comput. Fluids*, 2015, **107**, 214–223.
92 G. Li, G. H. McKinley and A. M. Ardekani, Dynamics of particle migration in channel flow of viscoelastic fluids, *J. Fluid Mech.*, 2015, **785**, 486–505.
93 A. H. Raffiee, S. Dabiri and A. M. Ardekani, Suspension of deformable particles in Newtonian and viscoelastic fluids in a microchannel, *Microfluid. Nanofluid.*, 2019, **23**(2), 22.
94 G. R. McNamara and G. Zanetti, Use of the Boltzmann equation to simulate lattice-gas automata, *Phys. Rev. Lett.*, 1988, **61**(20), 2332.
95 C. K. Aidun and J. R. Clausen, Lattice-Boltzmann method for complex flows, *Annu. Rev. Fluid Mech.*, 2010, **42**, 439–472.
96 C. K. Aidun, Y. Lu and E.-J. Ding, Direct analysis of particulate suspensions with inertia using the discrete Boltzmann equation, *J. Fluid Mech.*, 1998, **373**, 287–311.
97 E.-J. Ding and C. K. Aidun, The dynamics and scaling law for particles suspended in shear flow with inertia, *J. Fluid Mech.*, 2000, **423**, 317–344.
98 E.-J. Ding and C. K. Aidun, Extension of the lattice-Boltzmann method for direct simulation of suspended particles near contact, *J. Stat. Phys.*, 2003, **112**(3–4), 685–708.
99 T. Krüger, H. Kusumaatmaja, A. Kuzmin, O. Shardt, G. Silva and E. M. Viggen, *The Lattice Boltzmann Method: Principles and Practice*, Springer, 2016.
100 S. Succi, *The lattice Boltzmann equation: for fluid dynamics and beyond*, Oxford University Press, 2001.
101 A. J. Ladd, Numerical simulations of particulate suspensions via a discretized Boltzmann equation. Part 1. Theoretical foundation, *J. Fluid Mech.*, 1994, **271**, 285–309.
102 A. J. Ladd, Numerical simulations of particulate suspensions via a discretized Boltzmann equation. Part 2. Numerical results, *J. Fluid Mech.*, 1994, **271**, 311–339.
103 N.-Q. Nguyen and A. Ladd, Lubrication corrections for lattice-Boltzmann simulations of particle suspensions, *Phys. Rev. E: Stat., Nonlinear, Soft Matter Phys.*, 2002, **66**(4), 046708.
104 B. Chun and A. Ladd, Inertial migration of neutrally buoyant particles in a square duct: An investigation of multiple equilibrium positions, *Phys. Fluids*, 2006, **18**(3), 031704.
105 N. Nakagawa, *et al.*, Inertial migration of a spherical particle in laminar square channel flows from low to high Reynolds numbers, *J. Fluid Mech.*, 2015, **779**, 776–793.
106 C. Yuan, Z. Pan and H. Wu, Inertial migration of single particle in a square microchannel over wide ranges of Re and particle sizes, *Microfluid. Nanofluid.*, 2018, **22**(9), 102.
107 S. Dong-Ke, J. Di, X. Nan, C. Ke and N. Zhong-Hua, An immersed boundary-lattice boltzmann simulation of particle hydrodynamic focusing in a straight microchannel, *Chin. Phys. Lett.*, 2013, **30**(7), 074702.
108 W. Mao and A. Alexeev, Motion of spheroid particles in shear flow with inertia, *J. Fluid Mech.*, 2014, **749**, 145–166.
109 A. S. Jebakumar, K. N. Premnath and J. Abraham, Lattice Boltzmann method simulations of Stokes number effects on particle trajectories in a wall-bounded flow, *Comput. Fluids*, 2016, **124**, 208–219.
110 L. Zhang, A. S. Jebakumar and J. Abraham, Lattice Boltzmann method simulations of Stokes number effects on particle motion in a channel flow, *Phys. Fluids*, 2016, **28**(6), 063306.
111 W. Mao and A. Alexeev, Hydrodynamic sorting of microparticles by size in ridged microchannels, *Phys. Fluids*, 2011, **23**(5), 051704.
112 H. Başağaoğlu, P. Meakin, S. Succi, G. Redden and T. Ginn, Two-dimensional lattice Boltzmann simulation of colloid migration in rough-walled narrow flow channels, *Phys. Rev. E: Stat., Nonlinear, Soft Matter Phys.*, 2008, **77**(3), 031405.
113 D.-K. Sun and Z. Bo, Numerical simulation of hydrodynamic focusing of particles in straight channel flows with the immersed boundary-lattice Boltzmann method, *Int. J. Heat Mass Transfer*, 2015, **80**, 139–149.
114 T. Krüger, B. Kaoui and J. Harting, Interplay of inertia and deformability on rheological properties of a suspension of capsules, *J. Fluid Mech.*, 2014, **751**, 725–745.
115 D.-K. Sun, Y. Wang, A.-P. Dong and B.-D. Sun, A three-dimensional quantitative study on the hydrodynamic focusing of particles with the immersed boundary–Lattice Boltzmann method, *Int. J. Heat Mass Transfer*, 2016, **94**, 306–315.
116 A. Kilimnik, W. Mao and A. Alexeev, Inertial migration of deformable capsules in channel flow, *Phys. Fluids*, 2011, **23**(12), 123302.
117 Y.-L. Chen, Inertia-and deformation-driven migration of a soft particle in confined shear and Poiseuille flow, *RSC Adv.*, 2014, **4**(34), 17908–17916.
118 C. Prohm and H. Stark, Feedback control of inertial microfluidics using axial control forces, *Lab Chip*, 2014, **14**(12), 2115–2123.
119 C. Schaaf and H. Stark, Inertial migration and axial control of deformable capsules, *Soft Matter*, 2017, **13**(19), 3544–3555.
120 Z. Wang, Y. Sui, A.-V. Salsac, D. Barthès-Biesel and W. Wang, Motion of a spherical capsule in branched tube flow with finite inertia, *J. Fluid Mech.*, 2016, **806**, 603–626.
121 K. J. Humphry, P. M. Kulkarni, D. A. Weitz, J. F. Morris and H. A. Stone, Axial and lateral particle ordering in finite Reynolds number channel flows, *Phys. Fluids*, 2010, **22**(8), 081703.
122 S. Kahkeshani, H. Haddadi and D. Di Carlo, Preferred interparticle spacings in trains of particles in inertial microchannel flows, *J. Fluid Mech.*, 2015, **786**, R3.
123 W. Liu and C.-Y. Wu, Analysis of inertial migration of neutrally buoyant particle suspensions in a planar Poiseuille flow with a coupled lattice Boltzmann method-discrete element method, *Phys. Fluids*, 2019, **31**, 063301.
124 H. Haddadi and J. F. Morris, Topology of pair-sphere trajectories in finite inertia suspension shear flow and its effects on microstructure and rheology, *Phys. Fluids*, 2015, **27**(4), 043302.
125 C. Schaaf, F. Rühle and H. Stark, A flowing pair of particles in inertial microfluidics, *Soft Matter*, 2019, **15**(9), 1988–1998.
126 D. Jiang, W. Tang, N. Xiang and Z. Ni, Numerical simulation of particle focusing in a symmetrical serpentine microchannel, *RSC Adv.*, 2016, **6**(62), 57647–57657.

127 D. Di Carlo, D. Irimia, R. G. Tompkins and M. Toner, Continuous inertial focusing, ordering, and separation of particles in microchannels, *Proc. Natl. Acad. Sci. U. S. A.*, 2007, **104**(48), 18892–18897.
128 J. Matas, J. Morris and E. Guazzelli, Lateral forces on a sphere, *Oil Gas Sci. Technol.*, 2004, **59**(1), 59–70.
129 S. R. Risbud, M. Luo, J. Fréchette and G. Drazer, Analysis of the trajectory of a sphere moving through a geometric constriction, *Phys. Fluids*, 2013, **25**(6), 062001.
130 Z. Wu, Y. Chen, M. Wang and A. J. Chung, Continuous inertial microparticle and blood cell separation in straight channels with local microstructures, *Lab Chip*, 2016, **16**(3), 532–542.
131 D. Jiang, D. Huang, G. Zhao, W. Tang and N. Xiang, Numerical simulation of particle migration in different contraction–expansion ratio microchannels, *Microfluid. Nanofluid.*, 2019, **23**(1), 7.
132 H. Başağaoğlu, J. T. Carrola, C. J. Freitas, B. Başağaoğlu and S. Succi, Lattice Boltzmann simulations of vortex entrapment of particles in a microchannel with curved or flat edges, *Microfluid. Nanofluid.*, 2015, **18**(5–6), 1165–1175.
133 H. Haddadi and D. Di Carlo, Inertial flow of a dilute suspension over cavities in a microchannel, *J. Fluid Mech.*, 2017, **811**, 436–467.
134 H. Haddadi, H. Naghsh-Nilchi and D. Di Carlo, Separation of cancer cells using vortical microfluidic flows, *Biomicrofluidics*, 2018, **12**(1), 014112.
135 M. Jiang, S. Qian and Z. Liu, Fully resolved simulation of single-particle dynamics in a microcavity, *Microfluid. Nanofluid.*, 2018, **22**(12), 144.
136 R. Fattal and R. Kupferman, Constitutive laws for the matrix-logarithm of the conformation tensor, *J. Non-Newtonian Fluid Mech.*, 2004, **123**(2–3), 281–285.
137 H. Başağaoğlu, S. Succi, D. Wyrick and J. Blount, Particle Shape Influences Settling and Sorting Behavior in Microfluidic Domains, *Sci. Rep.*, 2018, **8**(1), 8583.
138 H. Başağaoğlu, J. R. Harwell, H. Nguyen and S. Succi, Enhanced computational performance of the lattice Boltzmann model for simulating micron-and submicron-size particle flows and non-Newtonian fluid flows, *Comput. Phys. Commun.*, 2017, **213**, 64–71.
139 H. Başağaoğlu, J. Blount, S. Succi and C. J. Freitas, Combined effects of fluid type and particle shape on particles flow in microfluidic platforms, *Microfluid. Nanofluid.*, 2019, **23**(7), 84.
140 X. Hu, J. Lin, D. Chen and X. Ku, Influence of non-Newtonian power law rheology on inertial migration of particles in channel flow, *Biomicrofluidics*, 2020, **14**(1), 014105.
141 S. C. Hur, N. K. Henderson-MacLennan, E. R. McCabe and D. Di Carlo, Deformability-based cell classification and enrichment using inertial microfluidics, *Lab Chip*, 2011, **11**(5), 912–920.
142 M. Villone, G. d'Avino, M. Hulsen and P. Maffettone, Dynamics of prolate spheroidal elastic particles in confined shear flow, *Phys. Rev. E: Stat., Nonlinear, Soft Matter Phys.*, 2015, **92**(6), 062303.

